RESEARCH ARTICLE OPEN ACCESS

Analysis Of Laminated and Sandwich Composites by A Zig-Zag Plate Element with Variable Kinematics and Fixed Degrees Of Freedom

Ugo Icardi*, Federico Sola**
*(Dipartimento di Ingegneria Meccanica e Aerospaziale, Politecnico di Torino, Italy)
** (Dipartimento di Ingegneria Meccanica e Aerospaziale, Politecnico di Torino, Italy)

ABSTRACT
A C° layerwise plate element with standard nodal d.o.f. and serendipity interpolation functions is applied to the analysis of laminates and sandwiches giving rise to strong layerwise effects. The element is obtained using an energy updating technique and symbolic calculus starting from a physically-based zig-zag model with variable kinematics and fixed d.o.f. able to a priori satisfy to displacement and stress continuity at the material interfaces. Non classical feature, a high-order piecewise zig-zag variation of the transverse displacement is assumed as it helps keeping equilibrium. Crushing of core is studied carrying apart a detailed 3D modelling of the honeycomb structure discretizing the cell walls with plate elements, with the aim of obtaining apparent elastic moduli at each load level. Using such apparent moduli, a 2D homogenized analysis is carried out simulating sandwiches as multi-layered structures Applications are presented to plates undergoing impulsive loading incorporating plies with spatially variable stiffness properties. It is shown that accurate predictions are always obtained in in the numerical applications with a very low computational effort. Compared to kinematically based zig-zag models, present physically based one is proven to more accurate, being always in a good agreement with exact 3D solutions.

Keywords **–** Impulsive loading, Indentation, Hierarchic representation, Optimized tailoring, Stress relaxation, Variable stiffness composites.

I. INTRODUCTION

Laminated and sandwich composites are increasingly finding use as they offer the possibility to optimize structural performances by properly choosing fibre orientation and stacking lay-up. These materials are widespread also owing to their high specific strength and stiffness, since they enable construction of structures that achieve the target requirements with the lowest mass possible (see, e.g. Sliseris and Rocens [1]).

Due to their inhomogeneous microstructure, unfortunately, they suffer from critical local stress concentrations that give rise to micro-damage formation and growth in service. Because elastic moduli and strengths in the in-plane direction are much bigger compared to those in the thickness direction, warping, shearing and straining deformations of the normal take place. A recent, comprehensive discussion about the mechanisms of damage formation and evolution and about their modelling is given by Càrdenas et al. [2]. As discussed by Chakrabarti et al. [3], Qatu et al. [4] and Zhang and Yang [5], these so called zig-zag and layerwise effects should be described with the maximal accuracy but with the lowest costs, in order to explore many possible design options with affordable costs.

Composite plate and shell theories and elements have been developed using different approaches. As examples of early theories, the papers by Wu and Liu [6], Cho et al. [7] and Averill and Yip [8] are cited. A review of such theories is presented in the paper by Burton and Noor [9]. An extensive discussion of the various techniques used to account for the layerwise effects and extensive assessments of their structural performances have been recently presented in the papers by Chakrabarti et al. [3], Matsunaga [10], Chen and Wu [11], Kreja [12], Tahani [13] and Gherlone [14]. In particular, accuracy of finite element models is assessed by Chakrabarti et al. [3], Zhang and Yang [5], Shimpi and Ainapure [15], Elmalich and Rabinovitch [16], Dau et al. [17], Feng and Hoa [18], Desai et al. [19], Ramtekkar et al. [20], To and Liu [21]. Zhen et al [22], Cao et al. [23] and Dey at al. [24].

Laminates and sandwiches with laminated faces constructed using automated fibre-placement technology (Barth [25]) whose reinforcement fibres follow curvilinear paths that are obtained using advanced optimization techniques achieve the maximal performance, as shown by Sousa et al. [26] and Honda et al. [27], and contemporaneously can relax critical local stress concentrations, as shown e.g. by Icardi and Sola [28]. Many iterations being

required by the optimization process, the use of efficient structural models that account for the zig-zag and layerwise effects with the minimal processing time and memory storage occupation becomes mandatory. Otherwise a mistaken prediction of these effects could result in inaccurate evaluations of strength, stiffness, failure behaviour and service life.

When a separate representation of layers is used, computational costs can become unaffordable for analysis and optimization of structures of industrial complexity, since the number of variables increases with the number of physical/computational layers. Models and elements based on a combination of global higher-order terms and local layerwise functions have been proven to be equally accurate but with a much lower computational effort (see, e.g. Elmalich and Rabinovitch [16] and the references therein cited). The Murakami's zig-zag function just based upon kinematic assumptions is often used as local layerwise function, but the assessments carried out by Gherlone [14] proven that it is accurate for periodical stack-ups, but not for laminates with arbitrary stacking sequences, or for asymmetrical sandwiches with high face-to-core stiffness ratios, like when a face is damaged.

On the contrary, physically-based zig-zag models have been proven to be always accurate. Refinements have been progressively brought to these models in order to achieve a good accuracy with the lowest computational burden and to successfully treat panels with low length-to-thickness ratio and abruptly changing material properties like sandwiches. To this purpose, sublaminate models having top and bottom face d.o.f. were developed by Aitharaju and Averill [29] and subsequently by other researchers in order to stack computational layers. The displacement field was recast in a global-local form to accurately predict stresses from constitutive equations (see, Li and Liu [30], Zhen and Wanji [31] and Vidal and Polit [32]), because post-processing operations are unwise for finite elements and cannot always give accurate results, as shown by Cho et al. [7]. Of course, sandwiches can be described as multi-layered structures assuming the honeycomb core as a thick intermediate homogeneous layer whenever a detailed description of local phenomena in the cellular structure is unnecessary (see, Phan et al. [33], Gibson and Ashby [34]).

The authors have recently developed a physically-based zig-zag model [35] aimed at carrying out the analysis of multi-layered and sandwich composites having abruptly changing properties with the minimal computational burden.

Its characteristic feature is a high-order piecewise zig-zag representation of the displacements that can be locally refined to obtain accurate stress predictions from constitutive relations, though its functional d.o.f. are fixed (the classical displacements and shear rotations of the normal at the mid-plane). Accurate results were obtained in the numerical applications with a computational effort comparable to that of equivalent single-layer models, thus considerably lower than for available layerwise models [35]. Symbolic calculus was used to obtain automatically and once for all in closed-form the relations required to a priori satisfy the physical constraints. In order to describe the core's crushing behaviour of sandwiches, a high-order piecewise zig-zag variation of the transverse displacement was assumed, while usually this is avoided in order to simplify algebraic manipulations. This representation also helps keeping equilibrium at cut-outs, free edges, nearby material/geometric discontinuities and to predict stresses caused by temperature gradients (see, e.g. [22] and [36]).

Regrettably, physically-based zig-zag models involve derivatives of the functional d.o.f., which thus should appear as nodal d.o.f. when developing finite elements. Consequently C1 or high-order representations are required, instead of computationally efficient C° interpolation functions. Techniques have been proposed for converting derivatives, but they result in an increase of the nodal d.o.f and thus of the memory storage dimension (see, e.g. Sahoo and Singh [37]). The energy updating technique [38] - [41], hereafter referred as SEUPT, originally developed as an iterative post-processing technique to improve the predictive capability of shear deformable commercial finite elements has been revised by the authors in [40] in order to obtain an equivalent C0 version of the zig-zag model [35] by the energy standpoint, which was used to develop an efficient eight node plate element.

In this paper, the finite element [40] is applied to study the indentation of sandwiches, to analyse the response of composite plates undergoing blast pulse loading and to consider the effects of variable-stiffness layers on the response of laminated and sandwich composites and on their stress fields. The numerical results are presented in the following sequence. Accuracy of the element is assessed comparing results for laminates with different stacking sequences, for sandwich plates and beams with asymmetric lay-ups, which give rise to strong layerwise effects, to exact three-dimensional solutions. As a further assessment, the collapse behaviour of honeycomb core will be studied using the element to discretize the cellular structure in details. Using the apparent elastic moduli varying with the load computed in this way, indentation studies are carried out in homogenized form discretizing sandwiches as multi-layered panels. In these cases, the comparison is made with experimental results from the literature. Finally, applications will be presented to plates undergoing

impulsive loading, which incorporate plies with spatially variable stiffness properties. The reasons for the choice of these samples cases are as follows.

Many studies investigating the core crushing mechanism have been presented in the literature where often a detailed finite element simulation of the cellular structure of honeycomb is adopted (Aminanda et al. [42]), because only in this way the buckling of cell walls can be accurately described. Solid elements are often used to discretize foam core (Mamalis et al. [43]). Crushing of core is followed by tearing of the loaded face. The topology of cells, their relative density and the thickness of the foil have considerable influence on this behaviour. Sandwiches being used as primary structures need an accurate simulations of these phenomena. However, despite accuracy could not always be maximal, in an industrial environment it is more attractive carrying out the simulations with advanced 2-D layerwise plate elements instead of using 3-D FEA and considering stress-based failure criteria instead of fracture mechanics or cohesive zone models (see, e.g., Panigrahi and Pradhan [44] and Menna et al. [45]), in order to keep affordable the computational burden. At the authors' best knowledge, no applications of last generation of refined zig-zag models and related elements have been still presented to indentation studies, in spite they could speed up simulations, saving computational costs and preserving accuracy.

To accurately describe crushing but with a low cost, in this paper the behaviour of core under transverse loading is determined apart once at a time by a finite element analysis where the cell walls are discretized by the present plate elements. In this way, the variation of the apparent properties of core under transverse loading are determined as apparent elastic moduli that vary with loading. The onset of damage is determined using stress-based criteria, but instead of considering a healthy material, a damaged material is considered at each iteration using the continuum damage mesomechanic model by Ladevèze et al. [46], [47]. This model provides a modified expression of the strain energy that accounts for the effects of the damage on the microscale, then stresses are computed taking into consideration the effects of local damage. The progressive failure analysis is carried out extending a pre-existing damage/failure to the points where the ultimate condition is reached, as predicted by stress-based criteria. Because the properties are assumed to vary with the applied load and from point to point over the contact area, the most relevant local phenomena in the core are considered. Once the apparent elastic properties of core have been determined, the analysis is carried out in 2-D form using elements [40], thus describing sandwiches as multi-layered plates.

As customarily, the indentation depth and the contact area are computed assuming the distribution of the contact force to be Hertzian and the projectile as a rigid body. The contact area is evaluated at any time step using the iterative algorithm by Palazotto et al. [48] that forces the surface of the target to conform to the shape of the impactor, as required by soft media. Because there is an equivalence between static and dynamic results for low velocity impacts, just a static simulation could be carried out. Nevertheless, the Newmark's implicit time integration scheme is employed to solve the transient dynamic equations, as it was developed to treat general transient dynamic problems of practical interest, as blast pulse loading.

In order to assess the potential advantages that could be obtained using variable stiffness composites, in particular whether a relaxation of critical stress concentrations can be obtained in practical test cases contemporaneously to a maximization of stiffness properties, the optimal property distributions computed by the tailoring optimization technique (OPTI) presented in Ref. [28] are used in the numerical applications. Using OPTI, the optimization problem of variable-stiffness composites turns into a simple problem of finding the appropriate stacking sequence, like with straight-fibre composites, which can be efficiently solved using the classical optimization techniques, because the optimal solution is computed apart once for all in closed or numerical form. As a consequence, a layerwise structural model can be used for having a realistic prediction of the structural behaviour without resulting into a unaffordable computational effort.

II. STRUCTURAL MODEL

The displacement field is assumed as the sum of four separated contributions [35]:

$$\begin{aligned} u(x,y,z) &= U^0(x,y,z) + U^i(x,y,z) + \\ &+ U^c(x,y,z) + U^{c\_ip}(x,y,z) \\ v(x,y,z) &= V^0(x,y,z) + V^i(x,y,z) + \\ &+ V^c(x,y,z) + V^{c\_ip}(x,y,z) \\ w(x,y,z) &= W^0(x,y,z) + W^i(x,y,z) + \\ &+ W^c(x,y,z) + W^{c\_ip}(x,y,z) \end{aligned} \tag{1}$$

whose purpose is explained hereafter. Symbols u, v and w respectively define the elastic displacements in the directions x, y and z of a rectangular Cartesian reference frame with (x, y) on the middle surface of the plate (Ω) and z normal to it.

A. Basic contribution Δ^0

Contributions with superscript^0 repeat the kinematics of the FSDPT model, as they contain just a linear expansion in z:

$$U^0(x,y,z)=u^0(x,y)+z\left[\gamma_x^0(x,y)-w^0{}_{,x}(x,y)\right]$$
$$V^0(x,y,z)=v^0(x,y)+z\left[\gamma_y^0(x,y)-w^0{}_{,y}(x,y)\right] \quad (2)$$
$$W^0(x,y,z)=w^0(x,y)$$

Displacements $u^0(x, y)$, $v^0(x, y)$, $w^0(x, y)$ and transverse shear rotations $\gamma_x{}^0(x, y)$ and $\gamma_y{}^0(x, y)$ at the middle plane represent the five functional d.o.f. of the model (1).

B. Variable kinematics contribution Δ^i

Contributions with superscript ^{i} are variable kinematic contributions that enable the representation to vary from point to point across the thickness, in order to refine the model where necessary:

$$U^i(x,y,z)=A_{x1}z+A_{x2}z^2+A_{x3}z^3+$$
$$+A_{x4}z^4+...+A_{xn}z^n$$
$$V^i(x,y,z)=A_{y1}z+A_{y2}z^2+A_{y3}z^3+ \quad (3)$$
$$+A_{y4}z^4+...+A_{yn}z^n$$
$$W^i(x,y,z)=A_{z1}z+A_{z2}z^2+A_{z3}z^3+$$
$$+A_{z4}z^4+...+A_{zn}z^n$$

The unknown coefficients A_{x1} … A_{zn} are computed as expressions of the functional d.o.f. and of their derivatives by enforcing conditions:

$$\sigma_{xz}|^u=0 \quad \sigma_{xz}|_l=0 \quad (4)$$
$$\sigma_{yz}|^u=0 \quad \sigma_{yz}|_l=0 \quad (5)$$
$$\sigma_{zz}|^u=p^0|^u \quad \sigma_{zz}|_l=p^0|_l \quad (6)$$
$$\sigma_{zz,z}|^u=0 \quad \sigma_{zz,z}|_l=0 \quad (7)$$

and the equilibrium at discrete points across the thickness:

$$\sigma_{xx,x}+\sigma_{xy,y}+\sigma_{xz,z}=0$$
$$\sigma_{xy,x}+\sigma_{yy,y}+\sigma_{yz,z}=0 \quad (8)$$
$$\sigma_{xz,x}+\sigma_{yz,y}+\sigma_{zz,z}=0$$

The symbols $^{(k)}z^+$ and $^{(k)}z^-$ were used to indicate the position of the upper$^+$ and lower $^-$ surfaces of the k^{th} layer and the superscript$^{(k)}$ the quantities that belong to a generic layer k. A comma was used to indicate differentiation.

The expressions of the unknowns A_{x1} … A_{zn} are obtained in closed-form as functions of the d.o.f. and of their derivatives using MATLAB® symbolic software package, thus they neither results into a considerably larger computational effort, nor into a larger memory storage. Because derivatives are unwise for the development of finite elements, the technique described forward and therein referred as SEUPT will be used to obtain a C° equivalent model.

It could be noticed that unknowns A_{x1} … A_{zn} can be determined also in order to fulfil boundary conditions such as clamped edges. It is reminded that assuming mid-plane displacements and shear rotations as functional d.o.f., when they are enforced to vanish in order to satisfy clamped constraints it automatically results that erroneous vanishing transverse shear stresses could be obtained. The successful application of the model to structures with clamped edges was shown in [35], [41] and [49]. A case will be also shown in this paper (Case B, section VI.B.2).

C. Zig-zag piecewise contribution Δ^c

These contributions, are assumed in the following form:

$$U^c(x,y)=\sum_{k=1}^{n_i}\Phi_x^k(x,y)(z-z_k)H_k+$$
$$+\sum_{k=1}^{n_i}C_u^k(x,y)H_k$$
$$V^c(x,y)=\sum_{k=1}^{n_i}\Phi_y^k(x,y)(z-z_k)H_k+ \quad (9)$$
$$+\sum_{k=1}^{n_i}C_v^k(x,y)H_k$$
$$W^c(x,y)=\sum_{k=1}^{n_i}\Psi^k(x,y)(z-z_k)H_k+$$
$$+\sum_{k=1}^{n_i}\Omega^k(x,y)(z-z_k)^2H_k+\sum_{k=1}^{n_i}C_w^k(x,y)H_k$$

They are aimed at making the displacements continuous and with appropriate discontinuous derivatives in the thickness direction at the interfaces of constituent layers, in order to *a priori* fulfil the continuity of interlaminar stresses at the material interfaces. Terms Φ_x^k, Φ_y^k are incorporated in order to satisfy continuity of transverse shear stresses:

$$\sigma_{xz}|_{(k)_{z^+}}=\sigma_{xz}|_{(k)_{z^-}} \quad (10)$$
$$\sigma_{yz}|_{(k)_{z^+}}=\sigma_{yz}|_{(k)_{z^-}}$$

while Ψ^k, Ω^k terms enable the fulfilment of continuity conditions:

$$\sigma_z|_{(k)_{z^+}}=\sigma_z|_{(k)_{z^-}} \quad (11)$$
$$\sigma_{z,z}|_{(k)_{z^+}}=\sigma_{z,z}|_{(k)_{z^-}}$$

which directly derive from the local equilibrium equations as a consequence of the continuity of transverse shear stresses.

Terms C_u^k, C_v^k and C_w^k restore the continuity of displacements at the points across the thickness where the representation is varied:

$$u|_{(k)_{z^+}}=u|_{(k)_{z^-}}$$
$$v|_{(k)_{z^+}}=v|_{(k)_{z^-}} \quad (12)$$

$$w\Big|_{(k)_{z^+}} = w\Big|_{(k)_{z^-}}$$

D. Variable in-plane representation Δ^{c_ip}

Contributions Δ^{c_ip} are incorporated in order to restore continuity when the material properties suddenly change moving along *x* or *y*:

$$\begin{aligned}
U^{c_ip} &= \sum_{j=1}^{S}\sum_{k=1}^{T} {}_u^j\theta_x^k(x,y)(x-x_k)H_k + \\
&+\sum_{j=1}^{S}\sum_{k=1}^{T} {}_u^j\theta_y^k(x,y)(y-y_k)H_k + \\
&+\sum_{j=1}^{S}\sum_{k=1}^{T} {}_u^j\lambda_x^k(x,y)(x-x_k)^2H_k + \\
&\sum_{j=1}^{S}\sum_{k=1}^{T} {}_u^j\lambda_y^k(x,y)(y-y_k)^2H_k + \ldots \\
V^{c_ip} &= \sum_{j=1}^{S}\sum_{k=1}^{T} {}_v^j\theta_x^k(x,y)(x-x_k)H_k + \\
&+\sum_{j=1}^{S}\sum_{k=1}^{T} {}_v^j\theta_y^k(x,y)(y-y_k)H_k + \\
&+\sum_{j=1}^{S}\sum_{k=1}^{T} {}_v^j\lambda_x^k(x,y)(x-x_k)^2H_k \\
&+\sum_{j=1}^{S}\sum_{k=1}^{T} {}_v^j\lambda_y^k(x,y)(y-y_k)^2H_k + \ldots
\end{aligned} \tag{13}$$

$$\begin{aligned}
U^{c_ip} &= \sum_{j=1}^{S}\sum_{k=1}^{T} {}_u^j\theta_x^k(x,y)(x-x_k)H_k + \\
&+\sum_{j=1}^{S}\sum_{k=1}^{T} {}_u^j\theta_y^k(x,y)(y-y_k)H_k + \\
&+\sum_{j=1}^{S}\sum_{k=1}^{T} {}_u^j\lambda_x^k(x,y)(x-x_k)^2H_k + \\
&\sum_{j=1}^{S}\sum_{k=1}^{T} {}_u^j\lambda_y^k(x,y)(y-y_k)^2H_k + \ldots \\
V^{c_ip} &= \sum_{j=1}^{S}\sum_{k=1}^{T} {}_v^j\theta_x^k(x,y)(x-x_k)H_k + \\
&+\sum_{j=1}^{S}\sum_{k=1}^{T} {}_v^j\theta_y^k(x,y)(y-y_k)H_k + \\
&+\sum_{j=1}^{S}\sum_{k=1}^{T} {}_v^j\lambda_x^k(x,y)(x-x_k)^2H_k \\
&+\sum_{j=1}^{S}\sum_{k=1}^{T} {}_v^j\lambda_y^k(x,y)(y-y_k)^2H_k + \ldots
\end{aligned} \tag{13a}$$

The exponent of $(x - x_k)^n$, $(y - y_k)^n$ is chosen in order to make continuous the gradient of order *n* of a stress component of interest. The expressions of all the continuity functions defined above are obtained once for all in a closed form by enforcing the fulfilment of the pertinent continuity conditions (Icardi and Sola [49]).

III. C0 EQUIVALENT MODEL AND FINITE ELEMENT

As well known, energy-based weak form versions of governing equations can be used to construct equivalent forms by the energy standpoint using various techniques. As shown by Icardi [38] and [39], an iterative post-processing technique working on a spline interpolation of results can be developed with the aim of constructing an updated solution that locally improves the accuracy of a finite element analysis by standard shear-deformable plate elements. In this way, accuracy can be improved up to the level of a layerwise model in the most critical regions, with a low computational effort.

The idea can also be used to derive a modified expression of the displacements fields by a structural model, in order to obtain a C^0 formulation free from derivatives to use for developing accurate and efficient finite element models, as shown by Icardi and Sola [39] - [41]. Applications of this technique, hereafter referred as SEUPT, to sample test cases with exact solutions and intricate through-the-thickness stress distributions, have shown that the equivalent model (EM) free from derivatives that is obtained from the consistent model (OM) of Eqs. (1)-(13a) is capable of providing results that are equally accurate, requiring a comparable low computational effort. The steps to develop an efficient finite element plate model with C° interpolation functions and standard nodal d.o.f. from the EM model are the following ones.

Hereon the displacements by the OM model will be indicated as $u(x,y,z)^{OM}$, $v(x,y,z)^{OM}$, $w(x,y,z)^{OM}$, their counterparts representing the equivalent C^0 model EM obtained by SEUPT will be indicated as $u(x,y,z)^{EM}$, $v(x,y,z)^{EM}$, $w(x,y,z)^{EM}$ or, in compact form, respectively as $\forall^{OM}$ and $\forall^{EM}$. In a similar way, all quantities by the OM model will be indicated with the superscript ^{OM}, while those referring to EM model with the superscript ^{EM}.

The basic assumption of SEUPT is that postulating displacements $\forall^{EM}$ as the sum of terms $\forall^{\varnothing}$ that are just functions of the d.o.f. and terms $\forall^{\cup}$ containing all the derivatives of the d.o.f.

$$\forall^{EM}(x,y,z) = \forall^{\varnothing}(x,y,z) + \forall^{\cup}(x,y,z) \tag{14}$$

each term $\forall^{\cup}$ can be replaced, since its energy contributions can be accounted for incorporating corrective terms free from derivatives Δu^0, Δv^0, Δw^0, $\Delta\gamma_x{}^0$, $\Delta\gamma_y{}^0$ (in compact form $\Delta\forall^{\varnothing}$):

$$\begin{aligned}
\forall^{EM}(x,y,z) &= \forall^{\varnothing}(x,y,z) + \\
&+\Delta\forall^{\varnothing}(x,y,z)
\end{aligned} \tag{14a}$$

thus an equivalent C° version EM of the zig-zag model OM can be obtained by the energy standpoint, which can be used to develop an efficient plate element. The expressions of $\forall^{\varnothing}$ are derived from the energy balance, which is written in compact form as:

$$\begin{aligned}
\delta\int(.)|_E &= \delta\int(.)|_{\Lambda i} - \delta\int(.)|_{\Lambda f} + \\
&+\delta\int(.)|_{\Lambda m} = 0
\end{aligned} \tag{15}$$

its three contributions being the strain energy, the work of external forces and the work of inertial forces, respectively.

To compute corrective terms $\forall^{\varnothing}$, the energy balance (15) is split into five independent balance equations, one for each primary variable, using the

principle of virtual work with the inertial forces accounted for, then each of these five contributions is further split collecting apart the single contributions of primary variables multiplying the same virtual displacement. The expressions of corrective terms $\forall^{\varnothing}$ are obtained equating each contribution by the OM model to its counterpart by the EM model:

$$\begin{aligned}
&\left[\delta\int(.)\,|_{E\longrightarrow}\right]^{u^0OM}=\left[\delta\int(.)\,|_{E\longrightarrow}\right]^{u^0EM}=0;\\
&\left[\delta\int(.)\,|_{E\longrightarrow}\right]^{v^0OM}=\left[\delta\int(.)\,|_{E\longrightarrow}\right]^{v^0EM}=0;\\
&\left[\delta\int(.)\,|_{E\longrightarrow}\right]^{w^0OM}=\left[\delta\int(.)\,|_{E\longrightarrow}\right]^{w^0EM}=0;\\
&\left[\delta\int(.)\,|_{\longrightarrow E}\right]^{\gamma_x{}^0OM}=\left[\delta\int(.)\,|_{E\longrightarrow}\right]^{\gamma_x{}^0EM}=0;\\
&\left[\delta\int(.)\,|_{E\longrightarrow}\right]^{\gamma_y{}^0OM}=\left[\delta\int(.)\,|_{E\longrightarrow}\right]^{\gamma_y{}^0EM}=0;
\end{aligned}\qquad(16)$$

Previous equations state that whether the consistent displacement fields by the OM model satisfy the energy balance, the modified displacements by the EM model satisfy it too, thus they represent an admissible solution by the energy standpoint. To solve once for all in closed form using symbolic calculus, appropriate spatial distributions of displacements under the same loading and boundary conditions should be postulated.

Assume that the domain Ω is decomposed into small generic quadrilateral subdomains Ω* The variation of the functional d.o.f. inside Ω* is expressed through Hermite's polynomials, since they represent the right interpolation scheme for developing a conforming element from the OM model. At least products of 5th order Hermite polynomials in *x* and *y* should be assumed because at least third-order derivatives in *x*, *y* are involved by the OM model. A regular solution is obtained in Ω by the superposition of solutions within subdomains Ω* because the Hermitian interpolation makes continuous the d.o.f. and their derivatives across adjacent subdomains. The purpose of SEUPT is to find a C^0 formulation represented by the equivalent EM model that allows for a computationally efficient Lagrangian representation, thus this type of representation is adopted in Eqs. (16) for the EM model. Because the continuity of displacement derivatives and stresses at sides and vertices of subdomains cannot be satisfied by the Lagrangian interpolation, it should be preliminary enforced in the OM model while computing terms Δ^{c_ip} of Eqs (13), (13a).

Because the EM model is just equivalent form the energy standpoint to the OM model, it only provides a correct solution in terms of displacement d.o.f. at any point, thus all the derived quantities like stresses should be computed by the OM model. Because expressions are obtained once for all via symbolic calculus, all updating operations and the computation of stresses are carried out in a very fast way requiring a very low computational effort in the numerical applications.

At this point, an efficient displacement-based, isoparametric C° plate element can be developed using standard techniques [39]. Because no derivatives are involved as nodal d.o.f., the vector of nodal unknowns can be assumed as:

$$\begin{aligned}
&\{Q\}=\\
&\left\{\left[u_1^o,v_1^o,w_1^o,\gamma_{x1}^0,\gamma_{y1}^0\right]^*,\left[u_2^o,v_2^o,w_2^o,\gamma_{x2}^0,\gamma_{y2}^0\right]^*,....,\right.\\
&\left.\left[u_8^o,v_8^o,w_8^o,\gamma_{x8}^0,\gamma_{y8}^0\right]^*\right\}^T
\end{aligned}\qquad(17)$$

(See inset in Figure 3). Consequently, standard serendipity Lagrangian interpolation functions can be used. At corners nodes (1, 2, 3, 4) they are expressed as:

$$N_i=\frac{1}{4}(1-\xi_{0i})(1+(-1)^{i-1}\eta_{oi})(\xi_{oi}\cdot(-1)^{i-1}\eta_{oi}-1)\qquad(18)$$

while at mid-side nodes (5, 6, 7, 8) they are expressed as:

$$\begin{aligned}
N_5&=\frac{1}{2}(1-\eta_{o5})(1-\xi_{05}{}^2)\\
N_6&=\frac{1}{2}(1-\eta_{o6}{}^2)(1+\xi_{06})\\
N_7&=\frac{1}{2}(1+\eta_{o7})(1-\xi_{07}{}^2)\\
N_8&=\frac{1}{2}(1-\eta_{o8}{}^2)(1-\xi_{08})
\end{aligned}\qquad(19)$$

Such a parabolic representation is chosen in order to obtain accurate results with a relatively coarse meshing, because accuracy of isoparametric four node quadrilateral elements can be too poor, as shown in the literature. It is reminded that no post-processing operations like integration of local differential equilibrium equations are required, since the stresses are accurately computed by the OM model from constitutive equations.

As customarily, mapping is used to standardize the computation of energy integrals, obtaining a square element with unit sides from any quadrilateral element in the physical plane

$$x=\sum_{i=1}^{8}x_iN_i\ \text{ and }\ y=\sum_{i=1}^{8}y_iN_i\qquad(20)$$

This isoparametric formulation allows to efficiently compute the Jacobian matrix

$$[J]=\begin{bmatrix}\dfrac{\partial x}{\partial\xi} & \dfrac{\partial y}{\partial\xi}\\ \dfrac{\partial x}{\partial\eta} & \dfrac{\partial y}{\partial\eta}\end{bmatrix}\qquad(21)$$

which is required to obtain the physical derivatives $\frac{\partial}{\partial x}$, $\frac{\partial}{\partial y}$ from the derivatives $\frac{\partial}{\partial \xi}$, $\frac{\partial}{\partial \eta}$ over the natural plane

$$\begin{Bmatrix} \frac{\partial}{\partial x} \\ \frac{\partial}{\partial y} \end{Bmatrix} = [J]^{-1} \begin{Bmatrix} \frac{\partial}{\partial \xi} \\ \frac{\partial}{\partial \eta} \end{Bmatrix} \quad (22)$$

The stiffness matrix is computed from the strain energy functional in the standard way as:

$$[K] = \int_{Ve} [B]^T [D][B] dV \quad (23)$$

the strains in infinitesimal form here considered being expressed as:

$$\{\varepsilon\} = [B]\{Q\} \quad (24)$$

and the stresses as:

$$\{\sigma\} = [D][B]\{Q\} \quad (25)$$

$[D]$ being the matrix of 3D elastic coefficients, Ve and the volume of the element.

The mass matrix is obtained from the kinetic energy functional as customarily:

$$[M] = \int_{Ve} \rho [N]^T [N] dV \quad (26)$$

ρ being the density. The vector of nodal loads is evaluated from the expression of the work of external forces in the standard way as:

$$\{Fe\} = \int_{Ve} [N]^T \{\bar{X}\} dV + \\ - \int_{Se} [N]^T \{\bar{f}\} dS - [N]^T \{\tilde{F}\} \quad (27)$$

$\{\bar{X}\}$ being the vector of body forces, $\{\bar{f}\}$ the vector of surface forces applied on the surface Se and $\{\tilde{F}\}$ the point forces. Integrations are carried out using a 3x3 Gaussian integrations scheme, since selective reduced integration is unnecessary because locking is avoided by a suited choice of coefficients Δ^i of the EM model and as a consequence of the present choice of the nodal d.o.f., since bending and transverse shear contributions are kept separated. The integrals are carried out summing up the contributions layer-by-layer when multilayered structures are considered.

IV. MODELLING OF LOADING AND DAMAGE

In this section, the techniques used for modelling blast pulse loading, the failure behaviour and indentation are overviewed.

A. Pulse pressure loading

When a pressure pulse is generated, a shock wave is transmitted in all directions. Once it reaches a structure, it creates a pressure wave characterized by an instantaneous pressure peak followed by a decrease as time folds. Research studies looking for configurations able to reduce the detrimental effects of such loading have been carried out by Gupta [50], Gupta et al. [51], Song et al. [52], Librescu et al. [53], [54] and Hause and Librescu [55] considering the overpressure $P_z(t)$ uniformly distributed over the whole panel, the front of the explosive blast pulse being supposed to be far, and its time variation expressed by Friedlander's exponential decay equation in modified form as:

$$P_z(t) = P_m \left(1 - \frac{t}{t_p}\right) e^{\left(-a' \frac{t}{t_p}\right)} \quad (28)$$

P_m being the overpressure peak, t_p the positive phase duration of the pulse measured from the time of impact and a' a decay parameter that is adjusted to approximate the pressure curve from the results of a blast test. A linear variation with an initial positive pressure peak that decays till to end with a negative pressure at the end of the overpressure phase is often considered in the numerical simulations to represent the sonic boom. Triangular, rectangular, step and sinusoidal pressure pulses are also often used, which are obtained as a particular case of previous equation. When the pressure pulse is idealized in this way, delay to pressure wave arrival, duration of pressure and maximum pressure are the parameters involved, which depend upon the offset distance between the point of explosion and the centre of the panel.

As refined structural models based on a combination of global higher-order terms and local layerwise functions like the present one were not considered in these studies, whether or not accurate modelling of layerwise and zig-zag effects can imply a considerable variation of results, i.e. a considerable mutation of best configuration able to resist to loading, still remains an open question that the present paper is aimed at contributing to discuss. To this purpose, sample cases presented in the literature will be retaken and analysed with the present structural model.

B. Solution of dynamic equations.

In this paper, the dynamic equations of the discretized structure under associated initial conditions:

$$\begin{cases} [M]\{\ddot{D}\}+[K]\{D\}=\{P(t)\} \\ \{D\}(0)=0 \\ \{\dot{D}\}(0)=0 \end{cases} \quad (29)$$

are solved using Newmark implicit time integration scheme, {D} being the vector of the nodal d.o.f. for the whole structure and {P(t)} the vector of nodal loads. Such solution scheme is chosen to solve the transient dynamic problem since explicit time integration is advantageous just when extremely strong geometric and material non-linearity are considered. This being not the present case, and since an explicit scheme need extremely small time steps to be stable, an implicit scheme was chosen. Accordingly, solution to Eqs. (29) is found representing the velocity and the acceleration vectors after a time step Δt as:

$$\{\dot{D}\}_{n+1}=\frac{\gamma}{\beta\Delta t}\left(\{D\}_{n+1}-\{D\}_n\right)+$$
$$+\left(1-\frac{\gamma}{\beta}\right)\{\dot{D}\}_n+\left(1-\frac{\gamma}{2\beta}\right)\Delta t\{\ddot{D}\}_n$$
$$\{\ddot{D}\}_{n+1}=\frac{1}{\beta\Delta t^2}\left(\{D\}_{n+1}-\{D\}_n\right)+$$
$$-\frac{1}{\beta\Delta t}\{\dot{D}\}_n+\left(1-\frac{1}{2\beta}\right)\{\ddot{D}\}_n \quad (30)$$

By substituting the expressions of Eq.(30) into Eq. (29), a linear algebraic solving system of the type $F(D_{n+1}) =0$ is obtained. In order to be unconditionally stable, the Newmark algorithm requires $2\beta \geq \gamma \geq 0.5$ (see, e.g. Ref. [28]). Aiming at meeting stability requirements, the calculations are carried out considering $\beta=1/4$ and $\gamma=1/2$, while for limiting convergence and rounding errors, relatively small time-steps are considered in this paper.

C. Indentation of sandwiches with honeycomb core

Because homogenized models cannot properly treat these collapsing mechanisms, a discrete modelling of honeycomb core giving a detailed representation of the real geometry is required. As microbuckling and local failure of core are highly mesh sensitive [56], a very refined meshing is required and a self-contact algorithm should be used to prevent from interpenetration between the folds in the cell walls.

In this paper a detailed, preliminary finite element analysis (PFEA) is carried apart once for all in order to compute the apparent elastic moduli of the core while it collapses/buckles under transverse compressive loading. In this phase, the present plate element is used to discretize the cell walls. An elastic-plastic behaviour [56] of the material constituting honeycomb walls is considered. The updated Lagrangian methodology is used to efficiently account for geometric nonlinearity.

Once the variable apparent elastic moduli are computed (as the tangent moduli derived from the average ratio of stresses and strains) the analysis is carried out in homogenized form by discretizing the sandwich panel as a multi-layered structure whose properties vary with the magnitude of indentation load and with position, as calculated by the PFEA phase. In this phase, geometric nonlinearity effects are accounted for still using the updated Lagrangian method. This approach is chosen since the discrete modelling of honeycomb may determine overloading computations when simulating structures of industrial complexity. The objective of numerical test will be that of assessing whether such modelling of the crushing behaviour of cells can be carried out separately from the homogenized analysis of the whole structure without a remarkable accuracy loss, in order to speed-up computations, as illustrated in Section VI.B.

As customarily, the indentation depth, the contact area and the contact stress are computed assuming the distribution of the contact force to be Hertzian. The projectile is described as a rigid body, while the nonlinear effective stiffness of the target structure, as it results by the finite element model including the plate stiffness and the contact stiffness, is employed for solving the contact problem. Non-classical feature, the contact radius and the applied pressure corresponding to the load are computed at each load step using an iterative algorithm (see, Palazotto et al. [48]) that forces the top surface of the target, i.e. the sandwich panel, to conform the shape of the impactor (in the least-squares sense) , the core being a soft media. At each time step, the contact radius is computed within each load step varying the displacements till the impacted top surface conforms to the shape of the impactor. The contact area radius computed at each load step is assumed as the estimated contact radius $R_{contact}$ for the next increment of load, which is used to compute the contact force according to the Hertzian law:

$$\sigma(r)=\sigma(0)\sqrt{1-\left(r^2/R_{contact}^2\right)}$$
$$(\sigma(r)=0 \text{ if } r>R_{contact}) \quad (31)$$

σ(r), σ(0) being the Hertzian stress intensity at a distance r from the centre coordinate and at the centre, respectively.

Initially, i.e. at the first time increment *Δt*, the contact force is assumed to reach the value *F=ΔF* and no damage is assumed to occur. The load is then iteratively incremented within the time-step, the contact area radius computed at each load step being assumed as the estimated contact radius for the next increment of load. The contact force *F* and the vertical displacement are computed when the shape of the target conforms to that of the impactor. In this way, the impactor moves on at a distance that depends upon the effective nonlinear stiffness of the panel. The damage is computed at each new time step as outlined forward, using the contact radius computed at the end of the previous load-step. The load is then incremented and the process repeated at the next time step till the impactor and the indentation radii are in agreement, then the failure analysis is performed again. Because the solution depends on the current configuration and previous history, the Newton-Raphson method is used to solve the contact problem. The residual force R_i is computed employing the secant stiffness matrix, the load at the next iteration $F_{(i)}$ and the solution at the previous iteration $q^0_{(i-1)}$, as customarily. The tangent stiffness matrix is used to evaluate the updated solution that makes the structure in equilibrium from the residual force balance. (see Figure 1)

Nevertheless there is a general agreement that for indentation studies there is a substantial equivalence between static and dynamic results, dynamic equations were solved in order to have the maximal accuracy, so to ascribe eventual discrepancies with reference solutions just to the present modelling approach.

D. Damage and failure

Stress-based criteria with a separate description of the various failure modes are here used to estimate the onset of the damage, as being simple enough and just requiring use of "engineering" variables they are suited to develop an efficient computational model. A mesoscale damage model is then employed for estimating the residual properties of the failed regions.

1) Onset of damage

The 3-D Hashin's criterion with in-situ strengths is chosen to predict the fibre's failure and the failure of the matrix. Tensile failure of fibres $(\sigma_{11} > 0)$ occurs if:

$$\left(\frac{\sigma_{11}}{X^t}\right)^2 + \frac{1}{S_{12=13}^{\ 2}}\left(\tau_{12}^{\ 2} + \tau_{13}^{\ 2}\right) = 1 \tag{32}$$

X^t being the tensile strength of fibres, $S_{12=13}$ the in-situ shear strength of the resin and σ_{11}, τ_{12}, τ_{13} the tensile and shear stresses acting on the fibres, while compressive failure $(\sigma_{11} < 0)$ of fibres occurs if:

$$\sigma_{11} = -X^c, \tag{33}$$

X^c being the compressive strength of fibres. The matrix failure under traction $(\sigma_{22} + \sigma_{33} > 0)$ is ruled by:

$$\left(\frac{\sigma_{22}+\sigma_{33}}{Y^t}\right)^2 + \frac{1}{S_{23}^{\ 2}}(\tau_{23}^{\ 2} - \sigma_{22}\sigma_{33}) + \\ + \left(\frac{\tau_{12}}{S_{12=13}}\right)^2 + \left(\frac{\tau_{13}}{S_{12=13}}\right)^2 = 1 \tag{34}$$

while under compression $(\sigma_{22} + \sigma_{33} < 0)$ by:

$$\frac{1}{Y^c}\left[\left(\frac{Y^c}{2S_{23}}\right)^2 - 1\right](\sigma_{22}+\sigma_{33}) + \\ + \frac{(\sigma_{22}+\sigma_{33})^2}{4S_{23}^{\ 2}} + \frac{(\tau_{23}^{\ 2} - \sigma_{22}\sigma_{33})}{S_{23}^{\ 2}} + \\ + \frac{(\tau_{12}^{\ 2} + \tau_{13}^{\ 2})}{S_{12=13}^{\ 2}} = 1 \tag{35}$$

The Choi-Chang's criterion is employed to predict the onset of delamination, which takes place if:

$$e_d^2 = D_a \left[\frac{\overline{\sigma}_{yz}^{\,n}}{S_i^n} + \frac{\overline{\sigma}_{xz}^{\,n+1}}{S_i^{n+1}} + \frac{\overline{\sigma}_{yy}^{\,n+1}}{Y_i^{n+1}}\right]^2 > 1 \tag{36}$$

where $Y^{n+1} = Y_t^{n+1}$ if $\overline{\sigma}_{yy} \geq 0$, or $Y^{n+1} = Y_c^{n+1}$ if $\overline{\sigma}_{yy} < 0$, D_a is an empirical constant that is set after consideration of the material properties, $\overline{\sigma}_{ij}$ is the average stress at the interface between the n^{th} ply and the $n+1^{\text{th}}$ ply, computed as follows:

$$\overline{\sigma}_{ij}^{n+1} = \frac{1}{h_{n+1}} \int_{t_{n-1}}^{t_n} \sigma_{ij}\, dt \tag{37}$$

The subscript '*i*' stands for *in situ*, while '*t*' and '*c*' stand for traction and compression, respectively. This criterion disregards the transverse interlaminar stress σ_{33}, but numerical tests in literature have shown that such omission is not relevant in the majority of cases, thus accurate estimations are usually obtained.

Crushing failure of with honeycomb core is predicted using the criteria by Besant et al. [57], Lee and Tsotsis [58] and Petras and Sutcliffe [59], in order to have the possibility of comparing different rules for this critical failure mode. The criterion by Besant et al. [57] uses the following expression:

$$\left(\frac{\sigma_{zz}}{\sigma_{cu}}\right)^n+\left(\frac{\tau_{xz}}{\tau_{lu}}\right)^n+\left(\frac{\tau_{yz}}{\tau_{lu}}\right)^n=e_{core} \quad (38)$$

to predicts failure, which occurs when $e_{core}>1$, σ_{cu} and τ_{lu} being the core strengths in compression and transverse shear. Numerical test in literature have shown that varying the exponent from 1 to 2 no remarkable effects appears on the results of sandwiches with laminated faces, but n = 1,5 best fitted the experimental results, thus this value was chosen. The criterion by Lee and Tsotsis [58] predicts indentation failure to occur at the loading magnitude at which one of these inequalities is verified:

$$\frac{\sigma_{zz}}{Z^c}=1\ ,\ \frac{\sigma_{xz}}{S^x}=1\ ,\ \frac{\sigma_{yz}}{S^y}=1 \quad (39)$$

Z^c, S^x, S^y being the compressive yield strength and the out-of-plane shear strengths, respectively. The criterion by Petras and Sutcliffe [59] predicts indentation failure when:

$$\frac{\sigma_{zz}}{Z^c}+\frac{(\sigma_{xz}+\sigma_{yz})}{S}=1 \quad (40)$$

S being the transverse shear strength.

2) Residual properties

The mesoscale damage model by Ladevèze et al. [47] is chosen for accurately computing the residual properties of failed structures, considering that this model and the other ones of the same class are known for being accurate and computationally more advantageous than structural scale models assuming cracks as hard discontinuities.

The discretely damaged medium is replaced with a continuous homogeneous medium, which is equivalent from an energy standpoint, whose strain energy expression incorporates damage indicators that are computed as the homogenized result of damage micro-models and have an intrinsic meaning. These damage indicators establish the link with the micro-degradation variables, namely they provide the relations giving the new elastic properties of the homogenized damaged model.

The homogenized potential energy density of a single layer assumed as the generic ply ^{S} is expressed as:

$$\frac{2E_p^S}{|S|}=[\pi\bar{\varepsilon}\pi]^t[\bar{M}_1(\bar{I}_{22},\bar{I}_{12})][\pi\bar{\varepsilon}\pi]+$$
$$+\tilde{\sigma}_{33}[\bar{M}_2(\bar{I}_{22},\bar{I}_{12})]\tilde{\sigma}_{33}+\tilde{\sigma}_{33}[\bar{M}_3(\bar{I}_{22},\bar{I}_{12})][\pi\bar{\varepsilon}\pi]+$$
$$-\frac{(1+\bar{I}_{23})\tilde{\sigma}_{23}^2}{\tilde{G}_{23}}-\frac{(1+\bar{I}_{13})\tilde{\sigma}_{13}^2}{\tilde{G}_{23}}-\frac{(1+\bar{I}_{33})<\tilde{\sigma}_{33}>_+^2}{\tilde{E}_3} \quad (41)$$

$\bar{I}_{22},\bar{I}_{12},\bar{I}_{23},\bar{I}_{13}$ and $\bar{I}_{33}$ being the five damage indicators defined as the integral of the strain energy of the elementary cell for each basic residual problem under the five possible elementary loads in the directions 22, 12, 23, 13,33. In the former equation $[\bar{M}_1]$, $[\bar{M}_2]$, $[\bar{M}_3]$ represent operators that depend on the material properties, $|S|$ is the deformation, while $<.>_+$ represents the positive part operator. Eq. (41) features an equivalent state of damage on the mesoscale that is approximately intrinsic for a given state of micro-degradation. Homogenization of the interface $|\gamma_j|$ leads to the following expression of the potential energy density:

$$\frac{2E_p^j}{|\gamma_j|}=-\frac{(1+\bar{I}^1)\tilde{\sigma}_{13}}{\tilde{k}_1}+$$
$$-\frac{(1+\bar{I}^2)\tilde{\sigma}_{23}}{\tilde{k}_2}-\frac{(1+\bar{I}^3)\tilde{\sigma}_{33}}{\tilde{k}_3} \quad (42)$$

$\tilde{k}_1$, $\tilde{k}_2$ and $\tilde{k}_3$ being the elastic stiffness coefficients of the interface, $\bar{I}^1$, $\bar{I}^2$ and $\bar{I}^3$ the three damage indicators and γ_j the deformation.

It is remarked that equations (41) and (42) are derived making the potential energy stored in the plies and in the interfaces the same as in the micromodel. In this way, a continuum damage model is constructed that is quasi-equivalent from an energy standpoint to the damage micro-model.

Solution is obtained as the sum of the solution of a problem $\tilde{P}$ in which damage is removed and the solution of a residual problem $\bar{P}$ where a residual stress is applied correcting the undamaged solution around each damaged area.

In the present paper, the residual problems for determining the expressions of damage indicators are solved numerically via 3D FEA discretization [60]. Once the damage indicators are computed, the expression of the strain energy is modified according to Eqs. (41), (42). Stresses are evaluated, then the failure criteria described in section IV.D.1 are used (at each time step in dynamic problems) to determine actual failed regions. In this way, the failure criteria are applied at any time step considering the materials damaged as in the reality.

The progressive failure analysis is carried out at the macroscopic level extending the pre-existing damage computed at the previous step to the points where the ultimate condition is reached, instead of

guessing factors for degrading the elastic properties of the failed regions like with the ply-discount theory.

V. VARIABLE-STIFFNESS COMPOSITES

Distributions of stiffness properties that minimize the energy absorbed involving out-of-plane strengths and, contemporaneously, that maximize the one absorbed by modes involving in-plane strengths are considered.

Such distributions are obtained once for all in closed or numerical form as variable ply angle distributions by solving the Euler-Lagrange equations obtained imposing extremal the in-plane, bending and out-of-plane shear contributions to strain energy under spatial variation of the stiffness properties [39], [41].

These candidate solutions represent in-plane variable-stiffness distributions making maximal or minimal the bending stiffness and increasing or decreasing interlaminar stresses, respectively. As a result, OPTI acts as an energy "*tuning*" procedure that transfer the incoming energy from out-of-plane critical modes to non-critical membrane ones (since laminates and sandwiches have larger strength and stiffness in the in-plane direction than in the thickness one), preserving a high bending stiffness. This non-classical optimization technique consists of the following steps.

First, the strain energy of the structural model is recast in a form that puts in evidence all terms Δ_{MN} function of elastic properties and of coefficients containing powers of z, which, once integrated across the thickness, define the stiffness properties of the model.

$$\delta\int(.)|_{\Lambda i}=\Pi=$$
$$\sum_{k=1}^{nl}\int_{z_{k-1}}^{z_k}\int_{\Omega}\left\{\sigma_{ij}\left(\Delta_{MN}\right)\right\}^{T}\left\{\varepsilon_{ij}\left(\Delta_{MN}\right)\right\}d\Omega dz \qquad (43)$$

Then, the first variation of former equation under variation of the stiffness properties is constructed, its vanishing enforced and the contributions of each functional d.o.f. are split apart (integration by parts) since the stationary conditions must hold irrespectively of the displacements

$$\delta\Pi=\int_{\Omega}\left[H\right]\left\{\delta D\right\}d\Omega \qquad (44)$$

[H] being a matrix containing the derivatives of the stiffness coefficients and {δ*D*} the column vector collecting the first variation of functional d.o.f. The contribution multiplying terms $\delta w^{(0)}$ is here referred as the strain energy due to bending, while the ones multiplying $\delta\gamma_x^{(0)}$, $\delta\gamma_y^{(0)}$ are referred as the strain energy due to transverse shears. Since contributions multiplying u^0 and v^0 are disregarded in the extremization process, as they represent in-plane uninteresting constraints a transfer of energy to in-plane mode being non-critical, just variations δw^0, $\delta\gamma_x^0$, $\delta\gamma_y^0$ require a simultaneous solution:

$$\sum H_{3j}=0;\sum H_{4j}=0;\sum H_{5j}=0 \qquad (45)$$

The spatial stiffness property distributions that make extremal the bending and transverse shear energy contributions are obtained solving the system of partial differential equations represented by (45) in terms of the stiffness properties, then finding appropriate ply-angle variations in closed or numerical form. The form of solutions is determined by the order of spatial derivatives of the stiffness coefficients in *x*, *y*. The present structural model gives rise to following variation of stiffness coefficients as general solution:

$$Q_{ij}=\sum_{p=1}^{P}\left[A_{1p}^{ij}e^{\left(px+{}^1\phi_n^x\right)}+{}^1k_x\right]\cdot\left[A_{2i}^{ij}e^{\left(py+{}^1\phi_n^y\right)}+{}^2k_y\right] \qquad (46)$$

(*ij*=11, 12, 13, 16, 22, 23, 26, 36, 44, 45, 55, 66). The unknown coefficients A_{1p}^{ij}, A_{2i}^{ij}, p, ${}^1\phi_x^n$, ${}^1\phi_y^n$, k_x, k_y are determined by enforcing conditions that determine whether the solution minimises or maximises the strain energy components, such as the stiffness at the bounds of the domain and a convex or a concave shape, as well as the thermodynamic constraints since the solution should be physically consistent.

Differently to former applications of the technique, here also the stiffness coefficients, Q_{44}, Q_{45} and Q_{55} are assumed to vary. However, their variation is very limited compared to the other coefficients as it will be shown forward, thus considering them as constants does not determine significant errors. If the properties of core are optimized across the thickness, the form of solutions is determined by the order of derivation in z and still has a similar general form like (46).

In the numerical applications, sub-optimal polynomial distributions

$Q_{ij}=\sum_{g=1}^{G}A_g x^g+B_g y^g$ will be considered, because they can be easily obtained with currently available automated fibre-placement manufacturing technologies. The numerical results will show how such sub-optimal stiffness distributions can be effective.

Three classes of variation of the stiffness properties over the surface of each single ply of this type will be considered, which are here named OPTI A, OPTI B and OPTI C. From the practical viewpoint, OPTI A maximizes the bending stiffness at the centre of the ply and makes it minimum at the edge. The in-plane variations of the most significant stiffness coefficients Q_{ij} for this case are reported in

Figure 2, from which it results that Q_{11} significantly increases at the centre of the ply, while it decreases at the edges. On the contrary, Q_{12}, that represents the local in-plane shear stiffness is higher at bounds of the ply, while at the centre it remains almost unchanged with respect to the straight fibre case. This variation is also the same of the coefficient Q_{22}.

The coupled effects of the distributions of Q_{11}, Q_{12} and Q_{22} produce an increase of the bending stiffness at the centre of the ply and a decrease at the bounds, while the shear stiffness does the opposite.

OPTI B also obtains a maximum bending stiffness at the centre of the ply and a low one at the edges, but the sign of the concavity imposed at the edge of the ply is different with respect to OPTI A. The global behaviour is roughly the same as for OPTI A, but a sharper variation is shown. Please notice that in this case the overall mean bending stiffness is almost similar to that of a straight fibre layer, thus OPTI B determines a lower increase of the bending stiffness with respect to OPTI A.

OPTI C obtains a maximum bending stiffness at the edge of the ply and a minimum one at the centre. In this case, the in-plane distribution Q_{11} is higher at the bounds than at the centre of the ply, while Q_{12} and Q_{22} behave in the opposite way and Q_{44} remains almost constant and similar to that of the straight fibre case. From the practical viewpoint OPTI C determines a transfer of energy from bending in the x-direction, to bending in the y-direction and to in-plane shear once incorporated into a laminate.

It could be observed that distributions OPTI A, OPTI B and OPTI C are similar to those obtained by other researchers using different optimization techniques (see, e.g. Refs. [61] and [62]). It will be shown that a suited combination of plies with these variable properties will consistently improve the structural performances of laminates and sandwiches, because the bending stiffness is kept maximal, while the deleterious concentrations of interlaminar stresses will be recovered. Of course, this latter effect is of primary importance by the viewpoint of durability and structural integrity, as the damage and failure mechanisms are dominated by the magnitude of interlaminar stresses.

VI. NUMERICAL APPLICATIONS

Accuracy and efficiency of the present structural model are assessed considering sample test cases of laminated and sandwich-like structures taken from the literature, whose exact 3D solutions are available. These structures are chosen due to their intricate through-the-thickness displacement and stress distributions consequent to extremely high length-to-thickness ratios, strong anisotropy or distinctly different/ abruptly changing asymmetric properties of constituent layers.

In details, applications will be presented to indentation of sandwiches with faces having distinctly different elastic properties, to [0°/90°/0°] simply-supported, thick cross-ply plates and [90°/0°/90°/0°], [0°/90°/0°/0°] laminated and sandwich beams in cylindrical bending (either undamaged or damaged) under sinusoidal transverse distributed loading, or subjected to pressure pulse loading and incorporating variable-stiffness plies, as discussed in section V.

Because numerical tests have shown that a reduced order of expansion of displacements (3) and an increased number of intermediate points at which equilibrium conditions (8) are enforced give better results, in all the numerical applications discussed next, for each physical layer a computational layers will be considered in the finite element analysis. It is reminded that with the present structural model subdivision into computational layers does not mean an increased number of unknowns, the functional d.o.f. of the model and the nodal d.o.f. being fixed, nevertheless the representation can be refined across the thickness.

A. Simply supported laminated and sandwich beams and plates

First extremely thick, simply supported sandwich beams and plates loaded by a sinusoidal transverse loading are considered.

1) Interlaminar stresses in [0°/90°/0°] plate under sinusoidal loading

The first case is that of a simply supported [0°/90°/0°] cross-ply plate. The constituent material has the following normalized mechanical properties: $E_L/E_T=25$; $G_{LT}/E_T=0.5$; $G_{TT}/E_T=0.2$; $\upsilon_{LT}=0.25$. Though unrealistic by the practical viewpoint, an overall length to thickness ratio of 4 is assumed, as it represent a severe test case. For this reason such case is often used by researchers for assessing accuracy of models. Simply supported edges and transversely distributed bi-sinusoidal loading acting on the top surface of the plate are considered, because under these conditions the exact 3D elasticity solution was found by Pagano [63]. The results for this case are reported in Figure 3 in normalized form as:

$$\bar{\sigma}_{xz}=\frac{\sigma_{xz}\left(0,\frac{L_y}{2},z\right)}{p^0 S} \qquad \bar{\sigma}_{yz}=\frac{\sigma_{yz}\left(\frac{L_x}{2},0,z\right)}{p^0 S} \tag{47}$$

In order to contain the length of the paper, it was chosen to represent just the interlaminar stresses because they are more difficult to capture than the in-

plane stresses and the displacements, as shown in the literature. In effects, many models can accurately predicts them only after integrating local differential equilibrium equations, not from constitutive equations.

Results for the other stresses and for the displacements will be reported and discussed next considering other test cases.

The results of Figure 3 show the capability of the finite element model to accurately capture shear stresses from constitutive equations with a reasonably refined, uniform meshing of 400 elements and in a rather efficient way. Indeed, the home-made computer code requires just 50 seconds to perform the analysis on a laptop computer with a 1800 GHz double-core processor and 2.96 GB RAM.

It could be noticed that results can be further refined till to become undistinguishable with respect to the exact solution without refining meshing, but instead by increasing the number of computational layers, as shown in Figure 3.

It is reminded that such refinement does not change the number of unknowns, it just imply a little increase of about 20% of the processing time.

2) Cross-ply and sandwich-like laminates in cylindrical bending

Table 1 reports a comparison of the results by the present finite element model with analytical solutions by other researchers [14] and with the exact elasticity solution [63], for several different cross-ply schemes and a sandwich-like structure.

The results reported in the table are the in-plane and out-of-plane displacements and the in-plane stresses at the points conventionally adopted for assessing structural models, as they were not considered in the previous test (VI.A.1). These quantities are important, though they do not intervene in the most critical failure mechanisms, because they directly represent the capability of the model to accurately predict the basic quantities. In the table are also reported the processing times by the present finite element model for each case (results under curly brackets).

Such results have been obtained considering a uniform meshing of the beams with 150 elements (see inset in Figure 4).

Case A. In the case of the [90°/0°/90°/0°] laminate, the constituent material MAT-p has the following mechanical properties: E_1 =25 GPa; E_2 = E_3 =1 GPa; G_{12}= G_{13}= 0.5; G_{23}=0.2; υ_{12}= υ_{13}= υ_{23}= 0.25. All the layers have thickness h/4, where h is the total thickness of the beam. Table 1 reports for different length-to-thickness ratios the comparison between the stress and displacement fields of the exact solution, those computed by the present element and those computed by Gherlone [14] using two first order theories adopting different zig-zag functions. Namely, the solution indicated as Gherlone PHYS employs a physically based zig-zag function, while that indicated as Gherlone MUR is obtained using a geometrically based zig-zag function. All the quantities are normalized as follows:

$$\bar{w} = \frac{L_y E_2}{q_0}\frac{(2h)^3}{L^4}\frac{1}{2h}\int_{-h}^{+h} w\left(\frac{L_x}{2}, z\right)dz$$

$$\left\{\bar{u}_{MIN}; \bar{u}_{MAX}\right\} = \frac{L_y E_2}{q_0}\frac{(2h)^2}{L^3}\begin{Bmatrix}\min\limits_{z\in[-h,+h]}\left[u(0,z)\right]\\ \max\limits_{z\in[-h,+h]}\left[u(0,z)\right]\end{Bmatrix} \quad (48)$$

$$\bar{\sigma}_{MIN} = \frac{L_y}{q_0}\left(\frac{2h}{L}\right)^2 \min_{z\in[-h,+h]}\left[\sigma_x\left(\frac{L_x}{2}, z\right)\right]$$

$$\bar{\sigma}_{MAX} = \frac{L_y}{q_0}\left(\frac{2h}{L}\right)^2 \max_{z\in[-h,+h]}\left[\sigma_x\left(\frac{L_x}{2}, z\right)\right]$$

The results shows the accuracy of the present finite element model even with a not extremely refined meshing, and more in general they show that using physically based zig-zag functions accuracy is dramatically better than for model using geometrically based one.

Case B. Same constituent material MAT-p are used for the [0°/90°/0°/0°] laminate. Because the thickness ratios of the layers currently are [0.1h/ 0.3h/ 0.35h/ 0.25h], the structure is strongly asymmetric and consequently the stress and displacement fields are asymmetric too. Different length-to-thickness ratios are considered also in this case. The results for this case still confirm the accuracy of the present finite element model with a rather coarse meshing and the improved accuracy achieved using a physically based zig-zag function, as shown by the comparison with its geometrically based counterpart by the results reported from [14].

Case C. The [0°/90°] lay-up is extensively used by researchers for assessing models since it is not a case easy to solve for the models. In effects, the correct evaluation of the stress and displacement fields for this structure is not a so trivial issue due to the strong unsymmetry of the lay-up and the extremely high thickness. Such effects require a refined modeling in order to accurately predict out-of-plane stresses from constitutive equations.

The present model and related element can easily treat this case because the representation can be refined across the thickness as desired without consistently increasing the computational effort and the stress-free boundary conditions at the upper and lower faces can be accounted for. The constituent layers still have the following mechanical properties: E_L/E_T=25; G_{LT}/E_T=0.5; G_{TT}/E_T=0.2; υ_{LT}=0.25. Figure 4 reports the stress and displacement field for this

case by Pagano [63] and by the present model normalised as follows:

$$\bar{\sigma}_x = \frac{\sigma_x\left(\frac{L_x}{2}, z\right)}{p^0}$$

$$\bar{\sigma}_z = \frac{\sigma_z\left(\frac{L_x}{2}, z\right)}{p^0} \qquad (49)$$

$$\bar{\sigma}_{xz} = \frac{\sigma_{xz}(0, z)}{p^0}$$

$$\bar{u} = \frac{E_T u(0, z)}{h p^0}$$

As a closure for this case it is remarked that the present finite element model is capable to reproduce with a high fidelity any quantity from the constitutive equations with a rather low computational effort (18.5 s) using a reasonably refined meshing. In particular, it is shown its capability to capture the strongly asymmetric variations of stresses, as well as the boundary conditions at the upper and lower faces.

Case D. The fourth structure considered is a sandwich-like beam, ideally made stacking three layers of MAT-p with altered properties. Namely, the mechanical properties of the second layer representing the core are reduced of a 10^5 factor, while those of the third layer representing the upper face starting from the bottom are reduced of the 20%. The thickness ratios of the constituent layers are [0.1h /0.7h /0.2h]. Due to the mechanical properties of the constituent material as well as to the stacking sequence, the laminate is again strongly asymmetric, thus it represents a severe test for the present element. Different length-to-thickness ratios are considered also for this case. It is shown again that the present element can obtain results as accurate as the exact 3D solution, as well as that the results obtained using a physically-based zig-zag function are significantly more accurate than those obtained using the Murakami's geometrically-based zig-zag function.

3) Undamaged and damaged sandwiches

The results presented next pertain sandwiches with honeycomb core, which either have undamaged or damaged properties, as displacement and stress fields are rather intricate and thus difficult to capture in the simulations.

Simply-supported edges and a sinusoidal distributed transverse loading are still considered, because the exact 3D solution is available for these cases. Results still refers to a length-to-thickness ratio 4.

Using the present element, the cellular structure of core could be discretized into details, but this is not currently done because the results used for comparisons have been determined considering the sandwich beam as a sandwich-like, multi-layered, homogenized structure where the core is described as a quite compliant intermediate thick layer and faces as thin, stiff layers. Instead, a detailed description of the cellular structure will be considered next studying indentation.

Case A. Four constituent materials are considered, whose mechanical properties are: MAT 1: E_1=E_3=1 GPa, G_{13}=0.2 GPa, υ_{13}=0.25; MAT 2: E_1=33 GPa, E_3=1 GPa, G_{13}=0.8 GPa, υ_{13}=0.25; MAT 3: E_1=25 GPa, E_3=1 GPa, G_{13}=0.5 GPa, υ_{13}=0.25; MAT 4: E_1=E_3=0.05 GPa, G_{13}=0.0217 GPa, υ_{13}=0.15. According to Aitharaju and Averill [64] who formerly studied the case, the lay-up is (Mat 1/2/3/1/3/4)$_s$ with the following thickness ratios of layers (0.010/0.025/0.015/0.020/0.030/0.4)$_s$. The face layers are made of three different materials indicated as MAT1 to MAT3, while the core is made of material MAT4. Compared each-others, the constituent materials have the following characteristics. Of course, the face layers are stiff, as customarily for a sandwich structures, while core is a light material that provides the necessary transverse shear stiffness. In details, MAT1 is rather weaker in tension-compression and shear, MAT2 is stiff in tension-compression and shear, while MAT3 is stiff in tension-compression, but rather compliant in shear. Being the core, MAT4 is compliant in tension-compression and rather compliant in shear.

Reduced stiffness properties of core are considered, which represent the degradation due to failure or damage accumulation, because they give rise to strongly steep-varying distributions, as shown by computing exact solutions with the technique [65] considering reduced elastic properties. In the present case, a factor 10^{-2} is considered for simulating the complete failure of the core under transverse shear (only G_{13} modulus of MAT4 reduced by factor 10^{-2}). The damage is assumed to be spread over the entire length of the sandwich beam, in order to have the possibility of finding the exact solution with the technique [63].

To contain the number of figures, hereon only partial sets of results are presented. Figure 5 reports the comparison between the exact solution [65] and the results by the present element, normalised as follows:

$$\bar{\sigma}_{xz} = \frac{\sigma_{xz}(0,z)}{p^0}$$
$$\bar{\sigma}_z = \frac{\sigma_z\left(\frac{L_x}{2},z\right)}{p^0} \qquad (50)$$
$$\bar{u} = 100\frac{u(0,z)}{hp^0}$$

The in-plane stress is omitted since it can be quite accurately captured even by equivalent single-layer models. As evidenced by the results, the variation of the transverse normal stress is correctly represented by the present finite element model. It could be noticed that in this case $\bar{\sigma}_z$ becomes as important as the transverse shear stress, the core being a rather "soft" material in compression under transverse loading. This implies that the assumption of a constant transverse displacement is inappropriate. The comparison with the exact solution having demonstrated that the representation of $\bar{\sigma}_z$ is correct, the variation of the transverse displacement necessary to construct such stress being automatically proven to be correct is not reported in order to contain the number of figures.

Also the in-plane displacement exhibits an intricate variation across the thickness that it is difficult to capture in the simulations. As a consequence, a refinement is required at the core interfaces which can be efficiently carried out by the present structural model without resulting neither into a larger memory storage occupation nor into a consistent increase of processing time, by increasing the number of computational subdivisions across the thickness in Eqs. (3)-(8).

Case B. As a further case with abruptly changing material properties, the sandwich with unsymmetric face layer properties and thus severe variation of stress gradients analysed by Brischetto et al. in [66] is now considered. The case examined is that of a simply supported, rectangular (L_y/L_x=3) sandwich plate with a length to thickness ratio of 4 undergoing bi-sinusoidal distributed loading.

The two skins are made of different material, their mechanical properties being: E_{ls}/E_{us}=5/4, $E_{ls}/E_c=10^5$, $\nu_{ls}=\nu_{us}=\nu_c=\nu=0.34$, where the subscript *ls* stands for lower skin, while *us* stands for upper skin, and *c* stands for core. Also the thickness of the layers are different being respectively h_{ls} =h/10; h_{us} =2h/10; h_c =7h/10 with respect to the thickness h of the plate. As a consequence of the high thickness ratio and mainly of these asymmetrical, distinctly different geometric and material properties, strong layerwise effects rise making this sample case a severe test for the model.

The results for this case are reported in Figure 6. A comparison is presented with the exact solution shown in [66] and the numerical results predicted by the present finite element model, by the numerical model considered in [66], which on the contrary of the present model is based upon use of Murakami's zig-zag function and a seventh order through-the-thickness representation. According to Ref. [66], stress and displacement are normalised as follows:

$$\bar{\sigma}_{xz} = \frac{\sigma_{xz}\left(0,\frac{L_y}{2},\mathrm{z}\right)h}{q^0 L_x}$$
$$\bar{u} = \frac{u\left(0,\frac{L_y}{2},\mathrm{z}\right)E_c h^2}{q^0 L_x^3} \qquad (51)$$

The results show that the present physically-based zig-zag model provides much more accurate results for the variation of the in-plane displacement across the thickness and only a little more accurate prediction of the shear stress, the reference model being already accurate for this quantity. As a concluding consideration, it can be seen that also for this case the present model gives results always in a very good agreement with the exact 3D solution at any point with still a reasonably refined in-plane meshing and low computational cost.

B. Indentation of sandwich plates

The behaviour of the "soft" material constituting the core needs to be accurately described, because a large amount of energy is absorbed through various folds and failure modes of the core structure. A micromechanics model with a very fine meshing was compared in [56] to a homogenized finite element model and to a homogenized discrete/finite element model. This latter model was shown to be the most appropriate for simulation of extensive core crushing, while it was observed that the homogenized model cannot always be successfully used.

Accordingly, in the present paper it was chosen to not explicitly model the honeycomb core and the faces using shell elements, but in order to save costs it was supposed that the analysis can be carried out using an homogenized model whose variable material properties with the loading magnitude are provided by the micromechanics model applied to a local analysis of some adjacent cell structures, as already mentioned above. So, a detailed, preliminary finite element analysis by the plate element of section (III) is carried apart once for all in order to describe the load-displacement curve of the core while it collapses/buckles under transverse compressive loading, the aim being to compute the apparent elastic moduli corresponding to each magnitude of the load. This analysis is carried out generating the

geometrical model of the sandwich structure in the finite element program RADIOSS^{TM} . Then, results are post-processed with the energy updating technique of section (III), in order to make them compatible with the OM model. In this context it should be noticed that the edges where cells are bonded each-others, the walls and the adhesive form a three-layer laminate that is appropriately treated by the OM model. Criteria of section (IV.D.1.) and the mesoscale model of section (IV.D.2.) are used in this phase to predict debonding failure at cell interfaces and fracture. Once the variable apparent elastic moduli are computed with the 3D model, the analysis is carried out in homogenized two-dimensional way just with an in-plane discretization by the elements of section (III). Namely, sandwiches are considered as laminated plates made of an equivalent material whose properties vary with the magnitude of the indentation load and with position over the plate. The updated Lagrangian method is still used to account for geometric nonlinearity effects.

The numerical result reported in the following section (VI.B.1) are presented in order to assess the correct implementation of the micromechanics 3D model of the cellular structure, those of section (VI.B.2) with the purpose to assess whether the collapse crushing failure analysis of sandwiches can be carried out in a homogenized 2D way as a plate whose variable properties are computed using the 3D model.

1) Three-dimensional model of crushing

It is now analysed the crushing behaviour of an aluminium alloy, honeycomb core. The square sandwich panel studied by Aminanda et al. [42] using a discrete modelling of the cellular structure is considered. The sample case treated has a cell size is of 6 mm, a cell wall thickness of 0,12 mm and a side length of the panel of 25 mm. The collapse analysis of core was carried out discretizing each cell wall into 150 plate elements, 25 elements being used in the direction across the thickness of the panel and 6 elements being used in the transverse direction, as shown in the inset of Figure 7.

Numerical results of Figure 7 show that once reached a peak of the indenting force, a sharp drop is presented because the cell walls rapidly buckle and cell folding starts, then the force is essentially transmitted to vertical edges.

Due to the progressive vertical edge deformation, after an initial linear elastic and stiff response, during this phase the force reaches a plateau and finally the diagram shows the condensation phase, where the stiffness restarts to increase. As it can be seen, the numerical results behave in accordance with the experiments [42], thus it is proven that the preliminary analysis of the collapse behaviour carried out by a discrete modelling of the cell walls is appropriately made using the plate element of section (III). The constituent material of cell walls being isotropic, all continuity functions (9) automatically vanish. Cell walls being very thin, the expansion order of the representation was limited to the first order contribution (2).

2) Two-dimensional overall model

Case A. It is now considered the sandwich square plate analysed by Flores-Johnson and Li [67] with a side-length of 100 mm. The plate has laminated [0°/90°] faces in Toho Tenax carbon fibre HTA plain weave fabric 5131, having the following mechanical properties $E_{11}= E_{22}=33,38$ GPa, $\upsilon_{12}=0,051$, $\sigma_{1T}= \sigma_{2T}=124$ MPa, $\sigma_{1T}= \sigma_{2T}=684$ MPa. The thickness of the faces is 0.416 mm.

Different constituent materials have been considered for the Rohacell foam cores: 51WF, 71WF, 110WF and 200WF. The mechanical properties of the foams are as follows: 51WF: $\sigma_C=$ 0.8 MPa, $\sigma_T=$ 1.6 MPa, E= 75 MPa, G= 24 MPa; 71WF: $\sigma_C=$ 1.7 MPa, $\sigma_T=$ 2.2 MPa, E= 105 MPa, G= 42 MPa; 110WF: $\sigma_C=$ 3.6 MPa, $\sigma_T=$ 3.7 MPa, E= 180 MPa, G= 70 MPa; 200WF $\sigma_C=$ 9 MPa, $\sigma_T=$ 6.8 MPa, E= 350 MPa, G= 150 MPa. The thickness of the core is 10 mm thick. The indentation is carried out considering a hemi-spherical indenter with 20 mm diameter.

A preliminary 3D analysis of the crushing collapse was carried out as outlined in the former section (VI.B.1). Then, the collapse analysis was carried out in 2D form. The results show a good agreement of these 2D simulation with the experimental results by Flores-Johnson and Li [67] everywhere except that for the strong oscillations of load- displacement curves at high deformation ratios. Excluding these regions, it could be noticed that the present 2D simulation is able to precisely capture the behaviour with, of course, a much lower computational effort than the 3D analysis, which however still shows some discrepancies where the reference experimental results oscillates. Please note that, in this case, 9994 elements have been considered during the 2D analysis, as shown by the insets reported in Figure 8. The computational times of this and subsequent case was seen to vary from 520 to 640 s.

Case B. To understand whether discrepancies with experiments repeats with other cases, the attention is now focused on the 139.7x139.7 mm sandwich panel with honeycomb core with different densities, studied by McQuigg [67]. Two sandwich panels are considered. The sample test case named in [67] as 3 PCF-XX has a Nomex^{TM} honeycomb core with density of 48.1 kg/m^3, 3.175 mm nominal cell size and 0.018 mm foil thickness, while those named 6 PCF-XX have Nomex^{TM} honeycomb core with

density of 96.11 kg/m^3, 3.175 mm nominal cell size and 0.038 mm foil thickness, respectively, while the thickness of the core is 12.7mm in both cases.

Both the panels have the skins made of two plies each of style 6781 woven S2-glass fabric cloth with 35% epoxy resin MTM45-1 content. The faces are 0.508 mm thick and their stacking sequence is [0°/45°]. In the warp direction strength and moduli are 561.65 MPa and 29 GPa, respectively, for tensile loading, and 575.23 MPa and 29 GPa, respectively, for compressive loading. In the fill direction strength and moduli are 555 MPa and 28 GPa, respectively, for compressive loading, and 476.22 MPa and 27.7 GPa, respectively, for tensile loading. The in-plane shear strength and modulus are 37.58 MPa and 3.79 GPa, respectively. The in-plane Poisson's ratio is 0.138. The indenter is a hemi-spherical indenter with 12,7 mm diameter and the panels are clamped on all four edges. In Figure 9 it is reported the comparison between the numerical results by the present element and the experimental ones by McQuigg [67]. In this case, both the analyses are carried out considering 4900 elements as shown by the insets reported in Figure 9. The comparison with [67] shows that rather accurate results are obtained, though the oscillations of the curves predicted by the present simulations are not perfectly replicating those of experiments in some regions. As discrepancies are rather small and similar to those shown in the literature, e.g. in [42] and [56], it is believed that all the essential phenomena are correctly described with the present modelling. It is left to a future study the investigation of the reasons of such discrepancies and whether a refined subdivision of the load-step used to carry out the analysis could improve accuracy.
Being at least as accurate as the other approaches presented in literature, the present modelling approach represents a good alternative to existing techniques for treating large sandwich structures of industrial interest keeping into account the local phenomena in the cellular structure with an affordable cost.

C. Laminates undergoing pulse pressure loading

Simply-supported plates subjected to blast pulse pressure loading are now considered. Initially, a laminated [0°/90°/0°] plate with a thickness ratio S=L/h of 4 and the layers of equal thickness (i.e., [h/3 / h/3 / h/3]) is considered, whose constituent layers have the following properties: $E_L/E_T=25$; $G_{LT}/E_T=0.5$; $G_{TT}/E_T=0.2$; $\upsilon_{LT}=0.25$. Then, layers with such straight-fibre orientation and so spatially uniform properties are replaced by variable-stiffness counterparts with curvilinear paths of fibres, as discussed in section V.

The lay-ups considered are of the following type: [0°/OPTI/90°/OPTI/0°], where OPTI represents a specific type of fibre angle variation. Several kinds of variable-stiffness distributions are considered, which are named OPTI 1 to OPTI 7. Each of these distributions is made of layers of type OPTI A, OPTI B or OPTI C, whose features are discussed in details in section V.

In details, OPTI 1 just considers layers of type OPTI C, OPTI 2 of type OPTI A, OPTI 3 layers of types OPTI C and OPTI A, OPTI 4 the opposite scheme, i.e. layers OPTI A - OPTI C, OPTI 5 layers of type OPTI B, while OPTI 6 is made of layers of types OPTI C and OPTI B and OPTI 7 does the opposite layers of types OPTI B and OPTI C being considered.

Figure 10 compares the deflection at the centre of the panel for all these lay-ups, as time unfolds under a triangular pulse loading [53] - [55], to the reference solution with uniform stiffness properties. The pressure is assumed constant over the panel, as in the cited references. In the numerical applications a density of 16.3136 Kg/m^3 was considered and $E_L=E_1=0.138$ GPa, assuming as side lengths $L_x=L_y=0.6096$ m.

Numerical, preliminary test have been carried out in order to assess the effects of the length-to-thickness ratio, obtaining as a result that the lower is this ratio, thus the higher are the layerwise effects, the lower is the amplitude of the oscillation and the higher is the frequency, as expected. Since a ratio of 4 is considered here, the deflection is much due to transverse shear than to bending, thus this case is suited for showing the effects of layers with variable-fibre orientation outside the usual range of thin plates, where their effectiveness on limiting bending have been already well focused.

Results on interlaminar stresses here not reported have shown that incorporation of OPTI plies considerably reduces the interlaminar stresses, without significant stiffness loss, confirming the result obtained in closed form in [39], [41], since path of fibres with variable orientation that try to minimize the bending component of the strain energy are coupled with ones that minimize the shear component of the strain energy. The best lay-ups by the viewpoint of deflections are OPTI 4 and OPTI 7, which are characterized by the simultaneous presence of plies that effectively minimize the bending component of the strain energy and of plies that minimize the shear component of the strain energy. The numerical results show that there are lay-ups among those considered with a lower amplitude of oscillations than other ones as time unfolds. Besides this fundamental effect by the practical viewpoint, the results show that due to low differences in the bending stiffness, the density being considered uniform as no variation is considered in the fibre volume fraction of solutions OPTI with respect to the straight-fibre case, small variation in the frequency,

or wave length occurs for the configurations examined.

The results being similar to those obtained in closed form in [39], [41], it is believed that present finite element model gave reasonable results also for the cases having no exact solutions available for comparisons.

D. Sandwich with local optimization

As a further test, the case with fibre paths that are interfaced with an angle that suddenly varies is considered in order to show whether the finite element obtains smooth results by virtue of the terms (13), (13a) incorporated in the structural model. In this case, a sandwich beam obtained interfacing face plies having variable-stiffness properties resulting from fibre paths that are differently oriented at the transition line is considered (see Figure 11a). It can be seen that the fibre distribution obtained in this way is characterized by an orientation angle that suddenly changes at the two interfaces x/ L_x = 1/3 and x/ L_x =2/3, while it smoothly varies elsewhere. In this case, the optimized distributions presented in Figure 2 are coupled into a single optimized layer, as shown in Figure 11a.

The results reported for this case are the variation of in-plane stresses moving in in-plane direction and of the transverse shear stress across the thickness under sinusoidal loading and for simply-supported edges.

The beam is characterized by a thickness ratio S of 10 and the properties of the un-optimized materials are: MAT FACE: E_1=25 GPa, E_3=1 GPa, G_{13}=0.5 GPa, υ_{13}=0.25; MAT CORE: E_1=E_3=0.05 GPa, G_{13}=0.0217 GPa, υ_{13}=0.15. The thickness of the layers is $(0.2/0.3)_s$, while the lay-up considered is reported in Figure 11a.

As a consequence of the fibre distribution adopted, the in-plane stress and its gradient become discontinuous at the two interfaces, as shown by the dashed line of Figure 11 if their continuity is not enforced crossing the interface. Through an appropriate definition of contributions (13), (13a) continuity is restored. It is worthwhile to mention that in this case, it is sufficient to consider continuity functions up to the third order in *x* in order to restore the in-plane continuity of the membrane stress and stress gradient, the difference between stiffness coefficients at the interfaces being rather mild.

Here the purpose is to show the capability of the finite element model to achieve continuous in-plane stress distributions across the interfaces of regions where the elastic properties suddenly change. This has a practical meaning because patches are used for repairing damage, or as a result of optimization studies aimed at achieving specific local properties when curvilinear paths of fibres are not used. A length-to-thickness ratio of 10 is considered, as it gives rise to sufficiently large bending deformations. The faces are assumed to be 2 mm thick, while the core is 6 mm thick.

In Figure 11a attention is focused on the bending stress while in Figure 11b the shear stress across the thickness is represented. These quantities are normalised as follows:

$$\bar{\sigma}_{xx} = \frac{\sigma_x\left(x, 0.4h\right)}{P}$$
$$\bar{\sigma}_{xz} = \frac{\sigma_{xz}\left(0, z\right)}{p^0} \tag{52}$$

From the through-the-thickness distribution of the transverse shear stress it could be noticed that the configuration reported in Figure 11a increases the maximum value of the shear stress in the faces, while it determines an appreciable decrease for the shear stress at the interface, which is the critical zone for the sandwich integrity.

VII. CONCLUDING REMARKS

Static and dynamic problems of laminated and sandwich structures were solved using a finite element model developed from a physically-based, 3D zig-zag plate model with variable kinematics and fixed degrees of freedom, which *a priori* fulfils the displacement and stress contact conditions at the material interfaces and the boundary conditions at the upper and lower bounding faces, as prescribed by the elasticity theory.

The virtues of this displacement-based structural model stem from the fact that its representation of displacements can be locally refined (either across the thickness, or in the in-plane directions), though its functional d.o.f. are fixed (the classical displacements and shear rotations of the normal at the mid-plane). Owing to such variable kinematics, accurate stress predictions are always obtained from constitutive relations even with extremely high length-to-thickness ratios, strong anisotropy, asymmetric stacking and distinctly different, abruptly changing properties of constituent layers, as well as nearby in-plane material/geometric discontinuities. Symbolic calculus was used to obtain automatically and once for all the expressions of continuity functions and high-order terms. A technique based on energy updating was used to convert the derivatives of the functional d.o.f., so that they do not appear as nodal d.o.f. in the finite element used in the analyses.

The main advantage of the C° finite element model obtained in this way is that analyses are carried out with the minimal computational burden, memory storage occupation and processing time being comparable to that of equivalent single-layer models.

Applications were presented to the study of indentation of sandwiches, to the analysis of the

response of composite plates undergoing blast pulse loading and to the analysis of benefits of variable-stiffness layers on the response of laminates and sandwiches and on their stress fields. The accuracy of present results were assessed considering laminates with different stacking sequences and sandwiches with laminated faces having intricate through-the-thickness displacement and stress distributions, either due to their extremely high length-to-thickness ratios, strong anisotropy or distinctly different/ abruptly changing asymmetric properties of constituent layers, for which exact solutions are available in the literature. In the cases where these solutions are not available, the present results were compared to experiments, like in the cases of analysis of the collapse behaviour of honeycomb core sandwiches with laminated faces subject to indentation loading.

The results confirm that accuracy of physically based zig-zag models is better than for of geometrically based zig-zag models, as shown in the literature. Indeed, the comparison with exact solutions shows that the present finite element model is always capable to reproduce with a high fidelity any quantity from the constitutive equations.

In particular, the results show the capability of the finite element model to always accurately capture out-of-plane stresses from constitutive equations with a reasonably refined meshing and in a rather efficient way for all the sample cases examined, as tens of seconds were required to perform the analysis on a laptop computer.

The analysis of sandwiches shows that even under transverse distributed loading with low magnitude the assumption of a constant transverse displacement is inappropriate, since as shown also by other studies in the literature the transverse normal stress becomes important for keeping equilibrium, the core being a rather "soft" material. The degradation due to failure or damage accumulation give rise to strongly steep-varying distributions that increase the importance of a correct representation of transverse displacement and stress. The effects of the degradation of properties, which by the viewpoint of elastic moduli represent cases of abruptly changing materials across the thickness, are captured with the right accuracy, owing to the capability of the zig-zag model of being refined across the thickness (still requiring tens of seconds to perform the analysis).

Indentation results show that apparent elastic moduli corresponding to each magnitude of the load while core collapses/buckles, can be computed apart and once for all without any accuracy loss through a detailed finite element analysis of the cellular structure of core. Apparent variable properties at any load level being preliminary computed apart, the analysis is subsequently carried out in homogenized form through an in-plane finite element discretization.

In this way, the simulations of structures of industrial complexity are speeded up, avoiding the overloading computations due to the detailed modelling of the cellular structure.

Incorporation of variable stiffness plies shows that lay-ups can be found that increase the bending stiffness and recover the transverse shear stress concentrations, as shown under static and blast pulse loading.

REFERENCES

[1] J. Sliseris, and K. Rocens, Optimal design of composite plates with discrete variable stiffness, *Composite Structures, 98*, 2013, 15 – 23.

[2] D. Càrdenas, H. Elizalde, P. Marzocca, F. Abdi, L. Minnetyan, and O. Probst, Progressive failure analysis of thin-walled composite structures, *Composite Structures*, *95*, 2013, 53-62.

[3] A. Chakrabarti, H.D. Chalak, M.A. Iqbal, and A.H. Sheikh, A new FE model based on higher order zig-zag theory for the analysis of laminated sandwich beam soft core, *Composite Structures*, *93*, 2011, 271-279.

[4] M.S. Qatu, R.W. Sullivan, and W. Wang, Recent research advances on the dynamic analysis of composite shells: 2000-2009, *Composite Structures, 93*, 2010, 14-31.

[5] Y. Zhang, and C. Yang, Recent developments in finite element analysis for laminated composite plates, *Composite Structures*, *88*, 2009, 147-157.

[6] C.P. Wu, and C.C. Liu, Mixed finite element analysis of thick doubly curved laminated shells, *J. Aerosp. Eng.*, *8*, 1995,43–53.

[7] M. Cho, K.O. Kim, and M.H. Kim, Efficient higher-order shell theory for laminated composites, *Composite Structures*, *34*, 1996, 197–212.

[8] R.C. Averill, and Y.C. Yip, An efficient thick beam theory and finite element model with zig-zag sublaminates approximations, *AIAA J.*, *34*, 1996, 1626-1632.

[9] W.S. Burton, and A.K. Noor, Assessment of computational models for sandwich panels and shells, *Comput. Methods Appl. Mech*., *123*, 1995,125-151.

[10] H. Matsunaga, A comparison between 2-D single-layer and 3-D layerwise theories for computing interlaminar stresses of laminated composite and sandwich plates subjected to thermal loadings, *Composite Structures, 64*, 2004, 161-177.

[11] W.J. Chen, and Z. Wu, A selective review on recent development of displacement-based laminated plate theories, *Recent Pat. Mech. Eng.*, *1*, 2008, 29–44.

[12] I. Kreja, A literature review on computational models for laminated composite and sandwich panels, *Central European Journal of Engineering*, *1*, 2011, 59 – 80.

[13] M. Tahani, Analysis of laminated composite beams using layerwise displacement theories, *Composite Structures*, *79*, 2007, 535-547.

[14] M. Gherlone, On the use of zigzag functions in equivalent single layer theories for laminated composite and sandwich beams: a comparative study and some observations on external weak layers, *J. of Appl. Mech.*, *80* (2013), 61004-1 – 61004-19.

[15] R.P. Shimpi, and A.V. Ainapure, A beam finite element based on layerwise trigonometric shear deformation theory, *Composite Structures*, *53*, 2011, 153-162.

[16] D. Elmalich, and O. Rabinovitch, A higher-order finite element for dynamic analysis of soft-core sandwich plates, *J. Sandwich Struct. & Mat.*, *14*, 2012, 525-555.

[17] F. Dau, O. Polit, and M. Touratier, C^1 plate and shell elements for geometrically nonlinear analysis of multi-layered structures, *Composite Structures*, *84*, 2006, 1264-1274.

[18] W. Feng, and S.V. Hoa, Partial hybrid finite elements for composite laminates, *Finite Elements in Analysis and Design*, *30*, 1998, 365-382.

[19] Y.M. Desai, G.S. Ramtekkar, and A.H. Shah, Dynamic analysis of laminated composite plates using a layer-wise mixed finite element model, *Composite Structures*, *59*, 2003, 237-249.

[20] G.S. Ramtekkar, Y.M. Desai, and A.H. Shah, Application of a three-dimensional mixed finite element model to the flexure of sandwich plate, *Comp. & Struct.*, *81*, 2003, 2183-2198.

[21] C.W.S To, and M.L. Liu, Geometrically nonlinear analysis of layerwise anisotropic shell structures by hybrid strain based lower order elements, *Finite Elements in Analysis and Design*, *37*, 2001, 1-34.

[22] W. Zhen, S.H. Lo, K.Y. Sze, and C. Wanji, A higher order finite element including transverse normal strain for linear elastic composite plates with general lamination configurations, *Finite Elements in Analysis and Design*, *48*, 2012, 1346 – 1357.

[23] C. Cao, A. Yu, and Q.-H. Qin, A novel hybrid finite element model for modelling anisotropic composites, *Finite Elements in Analysis and Design*, *64*, 2013, 36 – 47.

[24] P. Dey, A.H. Sheikh, and D. Sengupta, A new element for analysis of composite plates, *Finite Elements in Analysis and Design*, *82*, 2014, 62 – 71.

[25] J. Barth, Fabrication of complex composite structures using advanced fiber placement technology, *Proc. of 35th International SAMPE Symposium*, Anaheim, CA, 1990, 710-720.

[26] C.S. Sousa, P.P. Camanho, and A. Suleman, Analysis of multistable variable stiffness composite plates, *Composite Structures*, *98*, 2013, 34 – 46.

[27] S. Honda, T. Igarashi, and Y. Narita, Multi-objective optimization of curvilinear fiber shapes for laminated composite plates by using NSGA-II, *Composites: Part B*, *45*, 2013, 1071 – 1078.

[28] U. Icardi, and F. Sola, Response of sandwiches undergoing static and blast pulse loading with tailoring optimization and stitching, *Aerospace Science and Technology*, *32*, 2014, 293- 301.

[29] V.R. Aitharaju, and R.C. Averill, C^0 zig-zag finite element for analysis of laminated composites beams, *J. Eng. Mech.*, *125*, 1999, 323-330.

[30] X.Y. Li, and D. Liu, Generalized laminate theories based on double superposition hypothesis, *Int. J. Num. Meth. Eng.*, *40*, 1997, 1197–212.

[31] W. Zhen, and C. Wanji, A C^0-type higher-order theory for bending analysis of laminated composite and sandwich plates, *Composite Structures*, *92*, 2010, 653–661.

[32] P. Vidal, and O. Polit, A refined sine-based finite element with transverse normal deformation for the analysis of laminated beams under thermomechanical loads, *J of Mech of Materials and Struct.*, *4*, 2009, 1127-1155.

[33] C.N. Phan, Y. Frostig, and G.A. Kardomateas, Free vibration of unidirectional sandwich panels, Part II: Incompressible core, *J. Sandwich Struct. & Mat.*, 15, 2013, 412-428.

[34] L.J. Gibson, and M.F. Ashby, *Cellular solids: structure and properties. 2nd Edition* (Cambridge University Press, 1997).

[35] U. Icardi, and F. Sola, Development of an efficient zig-zag model with variable representation of displacement across the thickness, *J. Eng. Mech.*, 140, 2014, 531-541.

[36] U. Icardi, Multilayered plate model with "adaptive" representation of displacements and temperature across the thickness and

fixed d.o.f., *Journal of Thermal Stresses*, 34, 2011, 958–984.

[37] R. Sahoo, and B.N. Singh, A new shear deformation theory for the static analysis of laminated composite and sandwich plates, *Int. J. Mech. Sci., 75*, 2013, 324-336.

[38] U. Icardi, C^0 Plate Element for Global/Local Analysis of Multilayered Composites, Based on a 3D Zig-Zag Model and Strain Energy Updating, *Int. J. Mech. Sci.*, 47, 2005, 1561–1594.

[39] U. Icardi, Extension of the Strain Energy Updating Technique to a multilayered shell model with adaptive displacements and fixed DOF, *J. Aerosp. Eng.*, 26(4), 2013, 842-854.

[40] U. Icardi, and F. Sola, C0 fixed d.o.f. zig-zag model with variable in and out-of-plane kinematics and quadrilateral plate elements, Submitted to *J. Aerosp. Eng.*

[41] U. Icardi, and F. Sola, C^0 layerwise model with fixed d.o.f. and variable in and out-of-plane kinematics by SEUPT. " *Int. J. of Research Studies in Science, Engineering and Technology (IJRSST)*, 2014, IN PRESS

[42] Y. Aminanda, B. Castaniè, J.-J. Barrau, and P. Thevenet, Experimental analysis and modeling of the crushing of honeycomb cores, *Appl Compos Mater*, 12, 2005, 213-227.

[43] A.G. Mamalis, K.N. Spentzas, D.P. Papapostolou, and N Panteleis, Finite element investigation of the influence of material properties on the crushing characteristics of in-plane loaded composite sandwich panels, *Thin-Walled Structures*, *63*, 2013, 163-174.

[44] S.K. Panigrahi, and B. Pradhan, Onset and growth of adhesion failure and delamination induced damage in double lap joint of laminated FRP composites, *Composite Structures*, *85*, 2008, 326-336.

[45] C. Menna, D. Asprone, G. Caprino, V. Lopresto, and A. Prota, Numerical simulation of impact tests on GFRP composite laminates, *Int. J. Impact Eng.*, *38*, 2011, 677-685.

[46] P. Ladevèze, and G. Lubineau, On a damage mesomodel for laminates: micromechanics basis and improvement, *Mech. of Materials*, *35*, 2003, 763-775.

[47] P. Ladevèze, G. Lubineau, and D. Marsal, Towards a bridge between the micro- and mesomechanics of delamination for laminated composites, *Compos. Sci. & Tech.*, *66*, 2006, 698-712.

[48] A.N. Palazotto, E.J. Herup, and L.N.B. Gummadi, Finite element analysis of low-velocity impact on composite sandwich plate, *Composite Structures, 49*, 2000, 209-227.

[49] U. Icardi, and F. Sola, Analysis of bonded joints with laminated adherends by a variable kinematics layerwise model, *Int. J of Adhesion & Adhesives, 50*, 2014, 244–254.

[50] A.D. Gupta, Dynamic analysis of a flat plate subjected to an explosive blast, *Proc. of the ASME International Computers in Engineering Conference and Exhibition*, Boston, MA, 1985, 491–496.

[51] A.D. Gupta, F.H. Gregory, and R.L. Bitting, Dynamic response of a simply-supported rectangular plate to an explosive blast, *Proc. of SECTAM XIII: the South-eastern Conference on Theoretical and Applied Mechanics*, Columbia, SC, 1986, 385–390.

[52] O. Song, J.S. Ju, and L. Librescu, Dynamic response of anisotropic thin-walled beams to blast and harmonically oscillating loads, *Int. J. Impact Eng., 21(8)*, 1998, 663–682.

[53] L. Librescu, S.Y. Oh, and J. Hohe, Linear and non-linear dynamic response of sandwich panels to blast loading, *Composites: Part B, 35(6–8)*, 2004, 673–683.

[54] L. Librescu, S.Y. Oh, and J. Hohe, Dynamic response of anisotropic sandwich flat panels to underwater and in-air explosions, *Int. J. Solids Struct., 43(13)*, 2005, 3794–3816.

[55] T. Hause, and L. Librescu, Dynamic response of anisotropic sandwich flat panels to explosive pressure pulses, *Int. J. Impact Eng., 31(5)*, 2005, 607–628.

[56] L. Aktay, A.F. Johnson, and B. Kröplin, Numerical modeling of honeycomb core crush behavior, *Eng. Fracture Mech., 75*, 2008, 2616-2630.

[57] T. Besant, G.A.O. Davies, and D. Hitchings, Finite element modelling of low velocity impact of composite sandwich panels, *Composites: Part A, 32*, 2001, 1189-1196.

[58] S.M. Lee, and T.K. Tsotsis, Indentation failure behaviour of honeycomb sandwich panels, *Comp. Sci. & Tech., 60*, 2000, 1147–1159.

[59] A. Petras, and M.P.F. Sutcliffe, Indentation resistance of sandwich beams, *Composite Structures, 46*, 1999, 413–424.

[60] U. Icardi, and A. Atzori, Simple, efficient mixed solid element for accurate analysis of local effects in laminated and sandwich composites, *Advances in Eng. Software*, *32*, 2004, 843-849.

[61] M.A. Nik, K. Fayazbakhsh, D. Pasini, and L. Lessard, Optimization of variable

stiffness composites with embedded defects induced by Automated Fiber Placement, *Composite Structures*, *107*, 2014, 160-166.

[62] A. Khani, M.M. Abdalla, and Z. Gürdal, Circumferential stiffness tailoring of general cross section cylinders for maximum buckling load with strength constraints, *Composite Structures*, *94*, 2012, 2851 – 2860.

[63] N.J. Pagano, Exact solutions for rectangular bidirectional composites and sandwich plates, *J. Compos. Mater*., *4*, 1970, 20-34.

[64] V.R. Aitharaju, and R.C. Averill, C^0 zig-zag finite element for analysis of laminated composites beams, *J. Eng. Mech.*, *125*, 1999, 323-330.

[65] U. Icardi, Higher-order zig-zag model for analysis of thick composite beams with inclusion of transverse normal stress and sublaminates approximations, *Composites: Part B*, *32*, 2001, 343-354.

[66] S. Brischetto, E. Carrera, and L. Demasi, Improved response of asymmetrically laminated sandwich plates by using Zig-Zag functions, *J. Sandwich Struct. & Mat.*, *11*, 2009, 257- 267.

[67] E.A. Flores-Johnson, and Q.M. Li, Experimental study of the indentation of sandwich panels with carbon fibre-reinforced polymer face sheets and polymeric foam core, *Composites: Part B*, *42*, 2011, 1212-1219.

[68] T.D. McQuigg, *Compression After Impact experiments and analysis on honeycomb core sandwich panels with thin face sheets*, NASA/CR–2011-217157 NASA Langley Research Center Hampton, VA 23681-2199, 2011.

Table 1. Stress and displacement fields for laminated and sandwich-like beams by 3D elasticity solutions, by mixed elements with different kind of zig-zag functions and by the present element. Number in curly brackets are computational times in seconds.

CASE A - SIMPLY SUPPORTED [90°/0°/90°/0°] BEAM

L/2h	Model	$\bar{w}$	$\bar{u}_{max}$ z= -h	$\bar{u}_{min}$ z= +h	$\bar{\sigma}_{min}$ z= $^{(1)}z^{+}$	$\bar{\sigma}_{max}$ z=+h
8	Pagano [63]	0.0130	0.0290	-0.0150	-1.1380	1.2180
	Gherlone PHYS [14]	0.012852	0.026892	-0.014706	-1.127644	1.191691
	Gherlone MUR [14]	0.011202	0.020619	-0.013814	-1.06642	1.119342
	Present {18}	0.012864	0.027695	-0.014856	-1.132196	1.19973
L/2h	Model	$\bar{w}$	z= -h	z= +h	z= $^{(1)}z^{+}$	z=+h
14	Pagano [63]	0.0140	0.0240	-0.0140	-1.0580	1.1200
	Gherlone PHYS [14]	0.013924	0.023302	-0.013903	-1.054191	1.111488
	Gherlone MUR [14]	0.013072	0.021178	-0.01359	-1.032925	1.0864
	Present {13}	0.01393	0.0237	-0.013972	-1.056413	1.116304

CASE B - SIMPLY SUPPORTED [0°/90°/0°/0°] BEAM

L/2h	Model	$\bar{w}$	$\bar{u}_{max}$ z= -h	$\bar{u}_{min}$ z= +h	$\bar{\sigma}_{min}$ z= $^{(1)}z^{+}$	$\bar{\sigma}_{max}$ z=+h
8	Pagano [63]	0.0100	0.0120	-0.0100	-0.9570	0.7970
	Gherlone PHYS [14]	0.009512	0.011387	-0.01062	-0.905801	0.843784
	Gherlone MUR [14]	0.008728	0.013861	-0.008305	-1.10256	0.659836
	Present {18}	0.0098	0.011688	-0.0103	-0.936903	0.816527
L/2h	Model	$\bar{w}$	z= -h	z= +h	z= $^{(1)}z^{+}$	z=+h
14	Pagano [63]	0.0080	0.0130	-0.0100	-1.0090	0.7570
	Gherlone PHYS [14]	0.007815	0.012708	-0.01029	-0.985087	0.777818
	Gherlone MUR [14]	0.007418	0.013931	-0.009126	-1.080034	0.689778
	Present {13}	0.00788	0.012844	-0.01013	-0.998013	0.765706

CASE C - SIMPLY SUPPORTED SANDWICH-LIKE BEAM

L/2h	Model	$\bar{w}$	$\bar{u}_{max}$ z= -h	$\bar{u}_{min}$ z= +h	$\bar{\sigma}_{min}$ z= $^{(2)}z^{+}$	$\bar{\sigma}_{max}$ z=+h
8	Pagano [63]	1.1530	0.3110	-0.5790	-24.5270	24.5190
	Gherlone PHYS [14]	0.677388	0.207872	-0.208151	-13.11459	13.11767
	Gherlone MUR [14]	0.126138	0.037724	-0.034103	-2.975125	2.150316
	Present {21}	1.148388	0.3124	-0.574368	-24.77202	24.30127
L/2h	Model	$\bar{w}$	z= -h	z= +h	z= $^{(2)}z^{+}$	z=+h
24	Pagano [63]	0.6740	0.2010	-0.2020	-12.6920	12.7160
	Gherlone PHYS [14]	0.652836	0.198005	-0.19901	-12.50289	12.5278
	Gherlone MUR [14]	0.023388	0.018954	-0.014908	-1.496387	0.938441
	Present {19}	0.66389	0.199673	-0.201495	-12.5538	12.57755

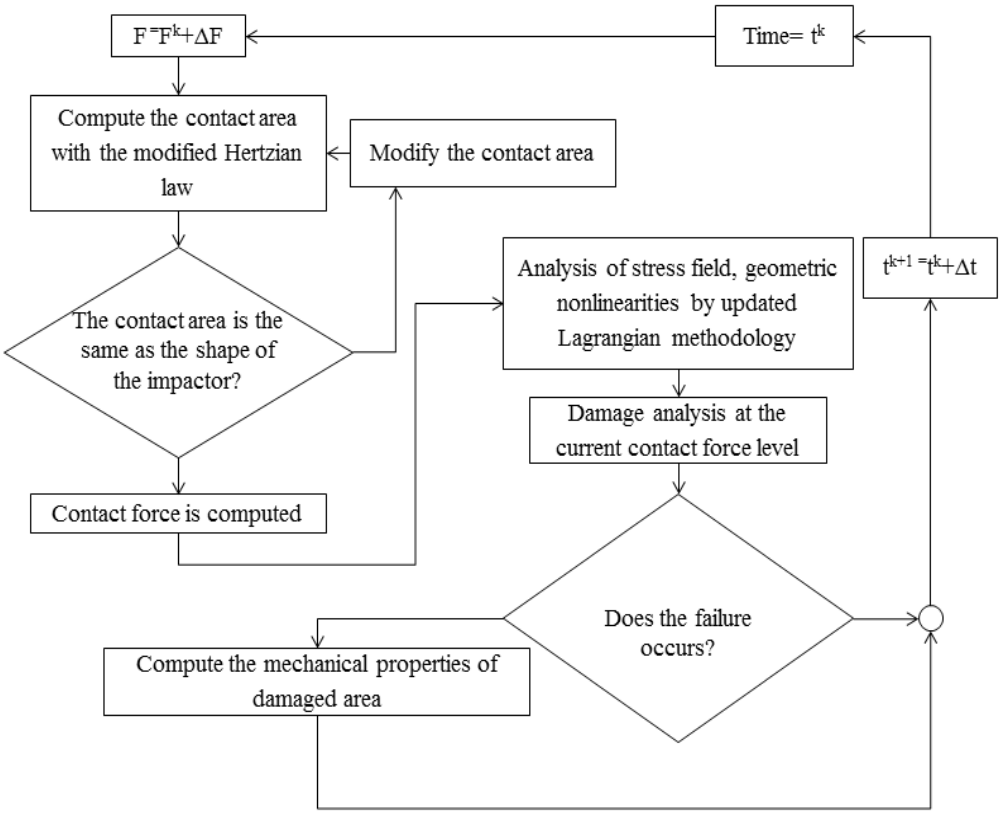

Figure 1. Stages of the procedure adopted to solve the indentation problem.

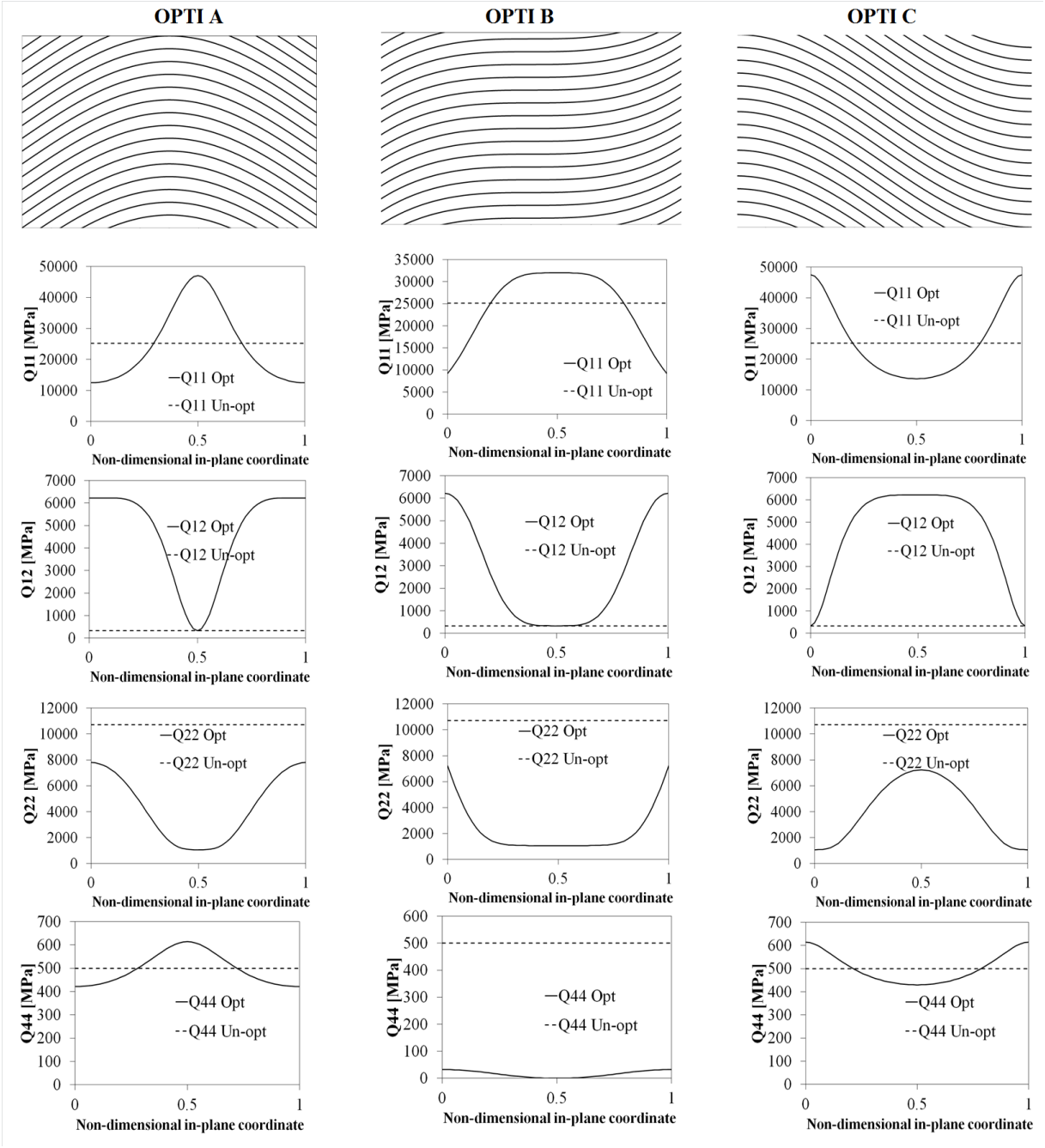

Figure 2. Optimized layers and in-plane variation of optimized Q_{ij}.

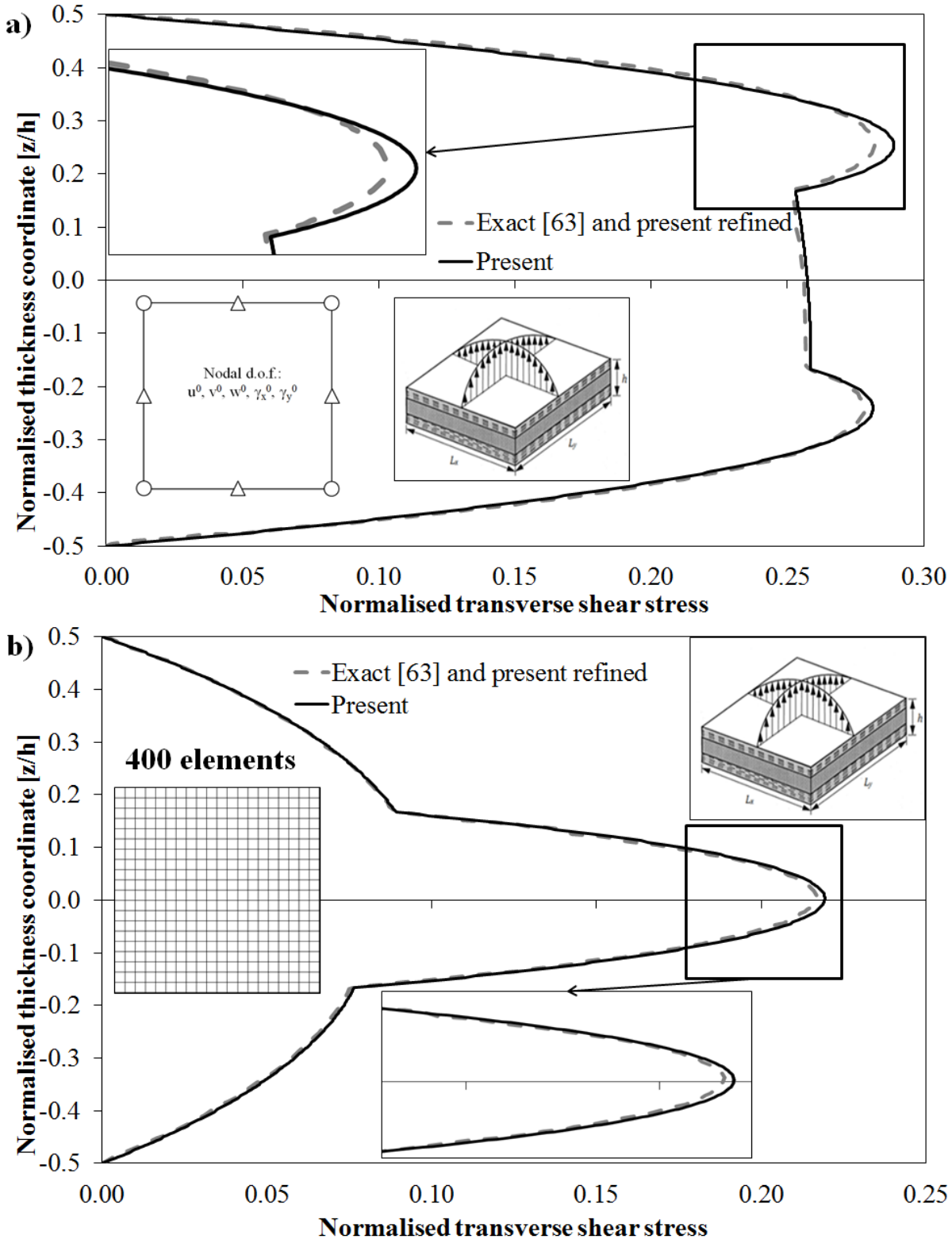

Figure 3. Comparison beetween solution by Pagano [63] (exact) and by the present model for a laminated [0°/90°/0°] plate: a) normalised transverse shear stress $\bar{\sigma}_{xz}$; b) normalised in-plane stress $\bar{\sigma}_{yz}$.

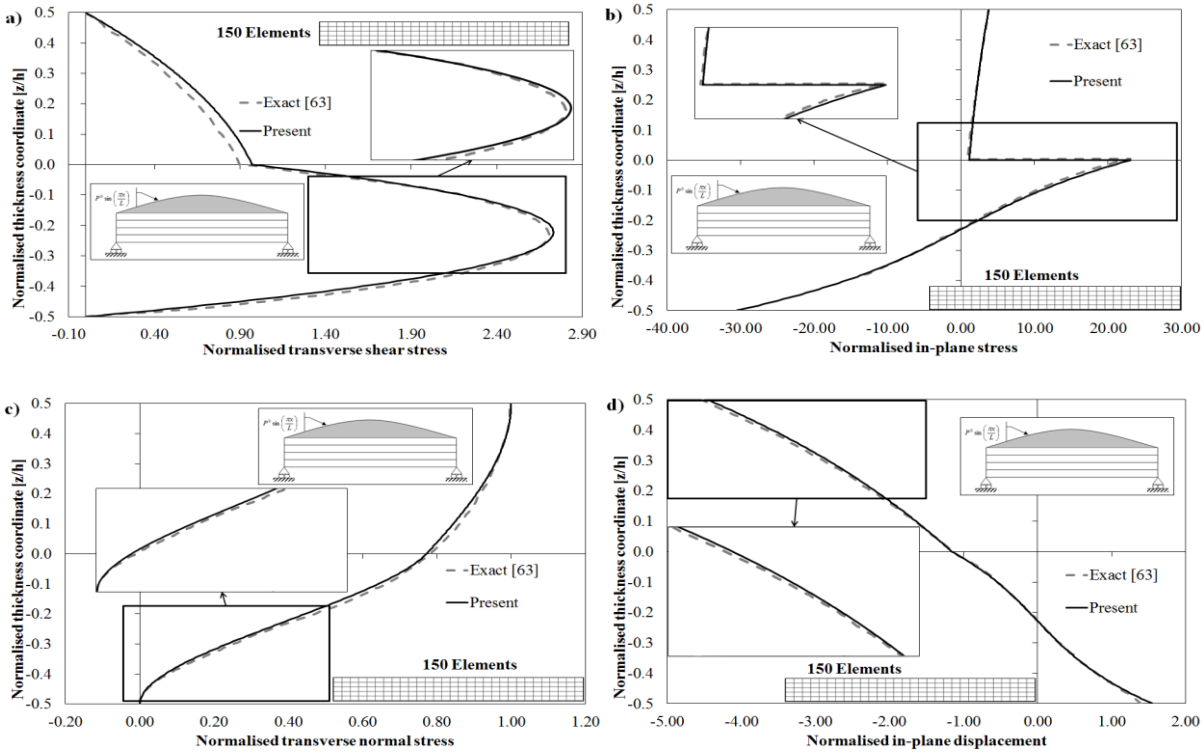

Figure 4. Comparison beetween solution by Pagano [63] (exact) and by the present model for a laminated [0°/90°] beam: a) normalised transverse shear stress; b) normalised in-plane stress; c) normalised transverse normal stress; d) normalised in-plane displacement.

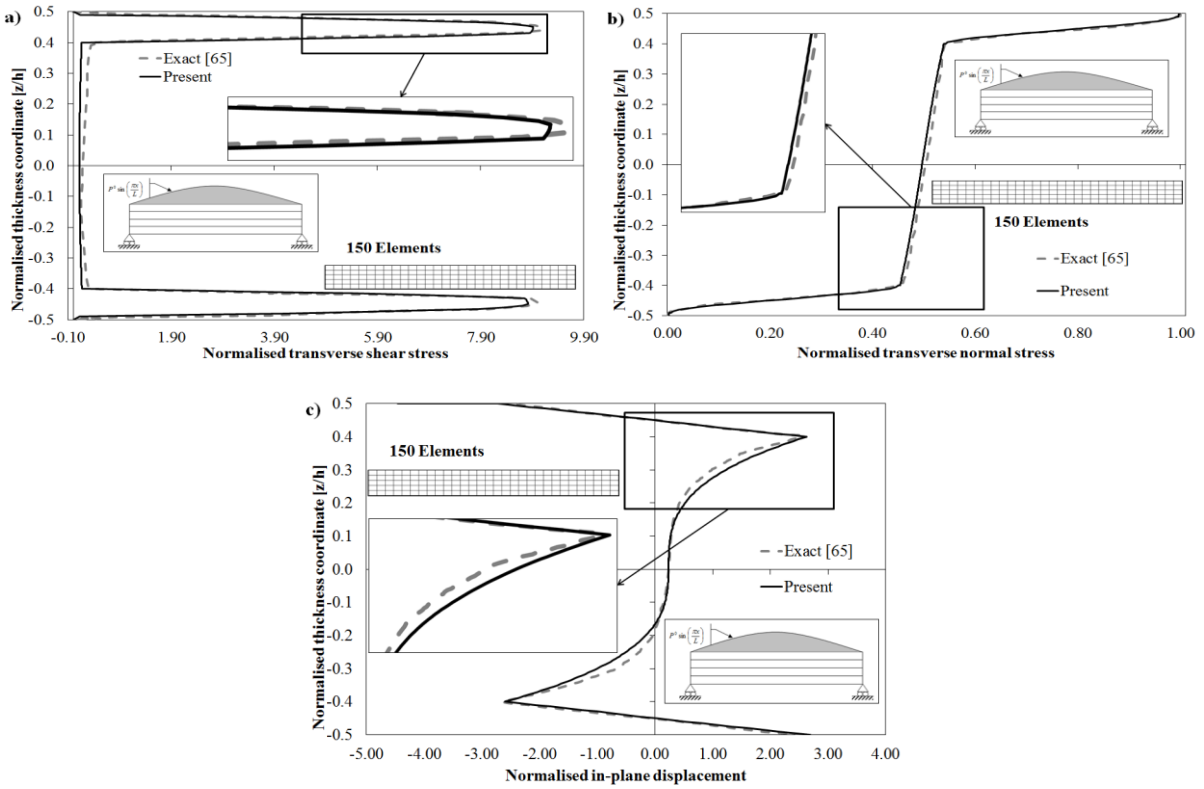

Figure 5. Comparison beetween exact solution [65] and solution by the present model for a sandwich beam with damaged core: a) normalised transverse shear stress; b) normalised transverse normal stress; c) normalised in-plane displacement.

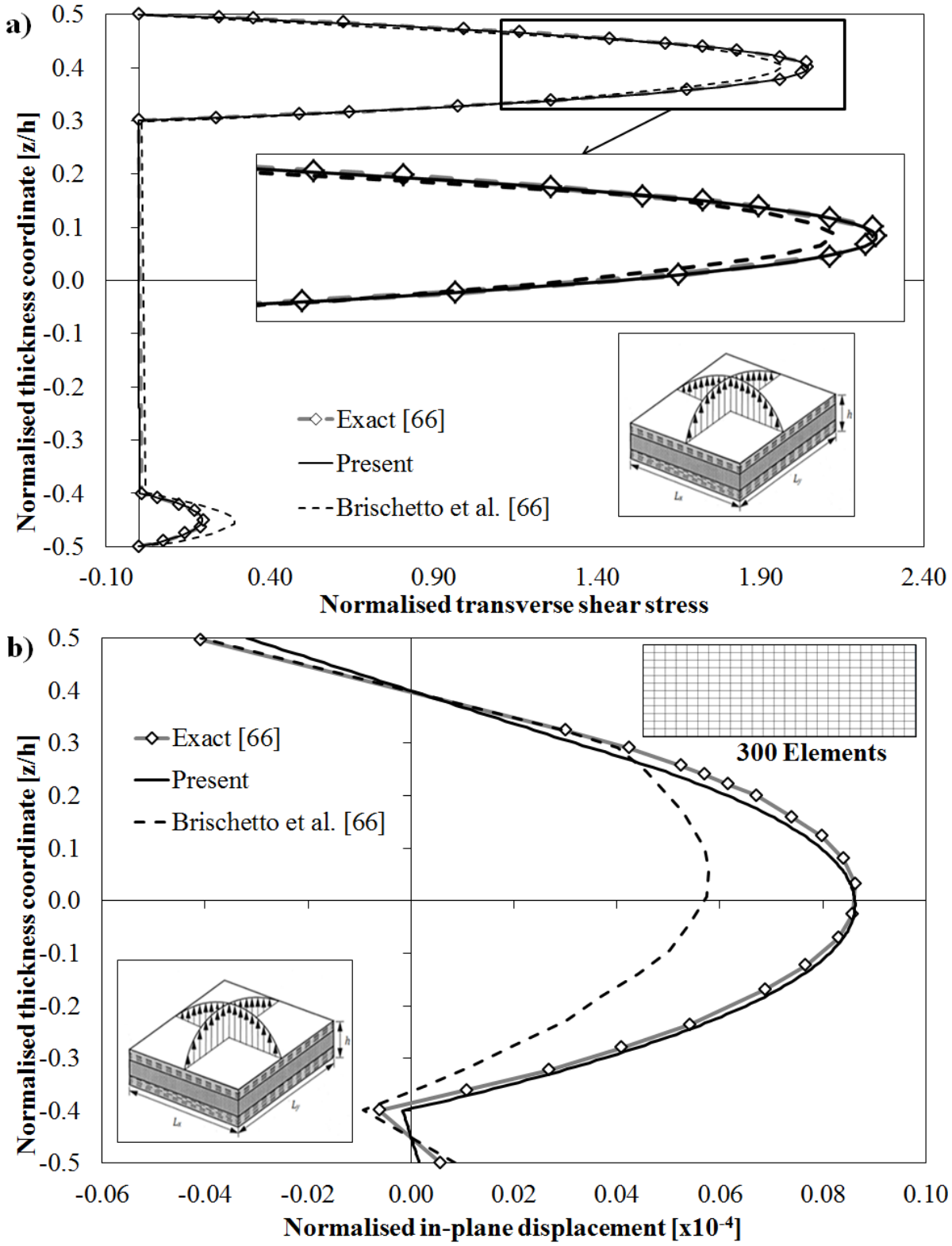

Figure 6. Transverse shear stress and transverse displacement for a sandwich plate by Brischetto et al. [66] (exact 3D solution and FEM solution) and by the present finite element.

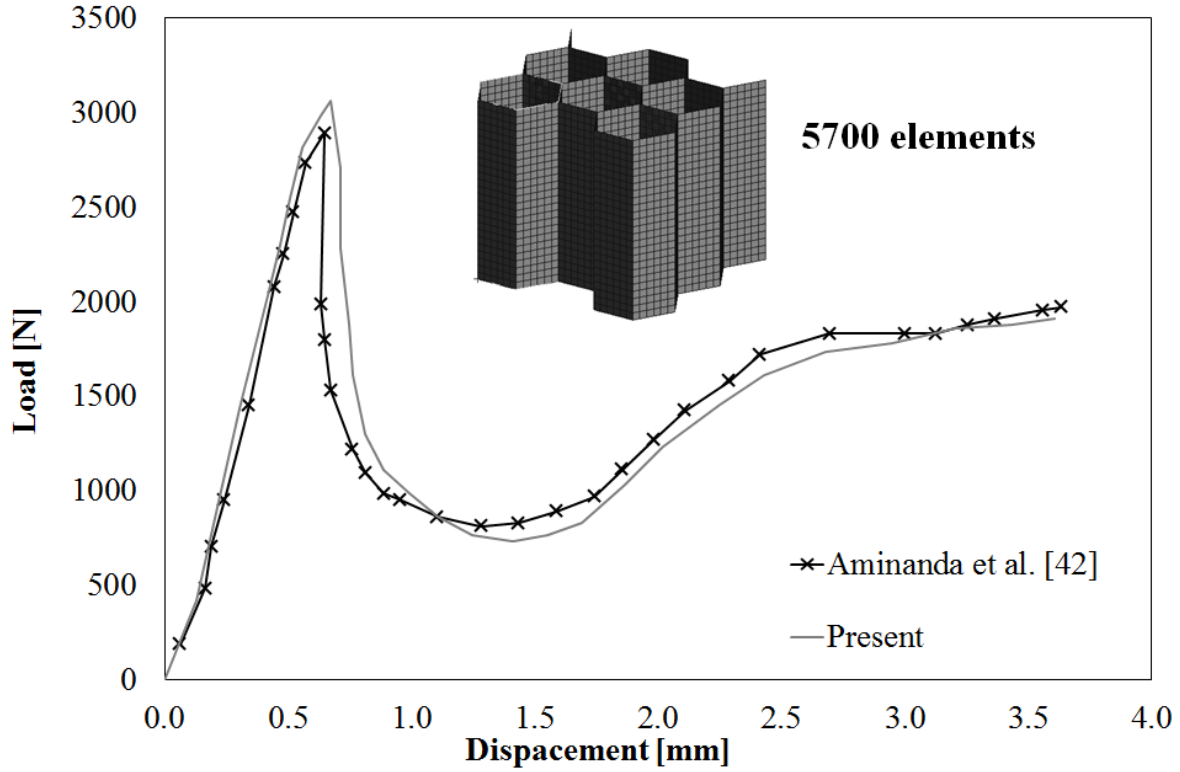

Figure 7. Crushing behaviour for an aluminium honeycomb by Aminanda et al. [42] (experiment) and by the present element.

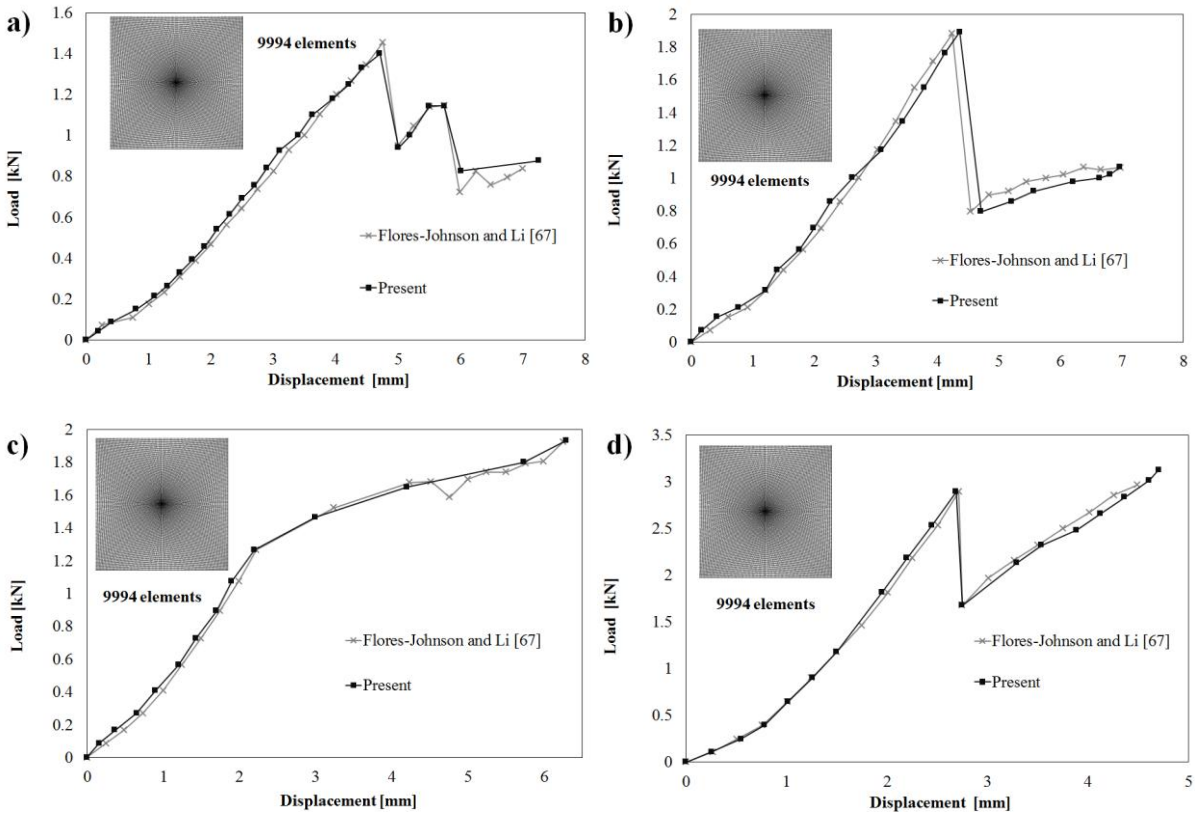

Figure 8. Experimental [67] and present force-indentation curves for sandwich plates with a) 51WF foam core, b) 71WF foam core, c) 110WF foam core and d) 200WF foam core.

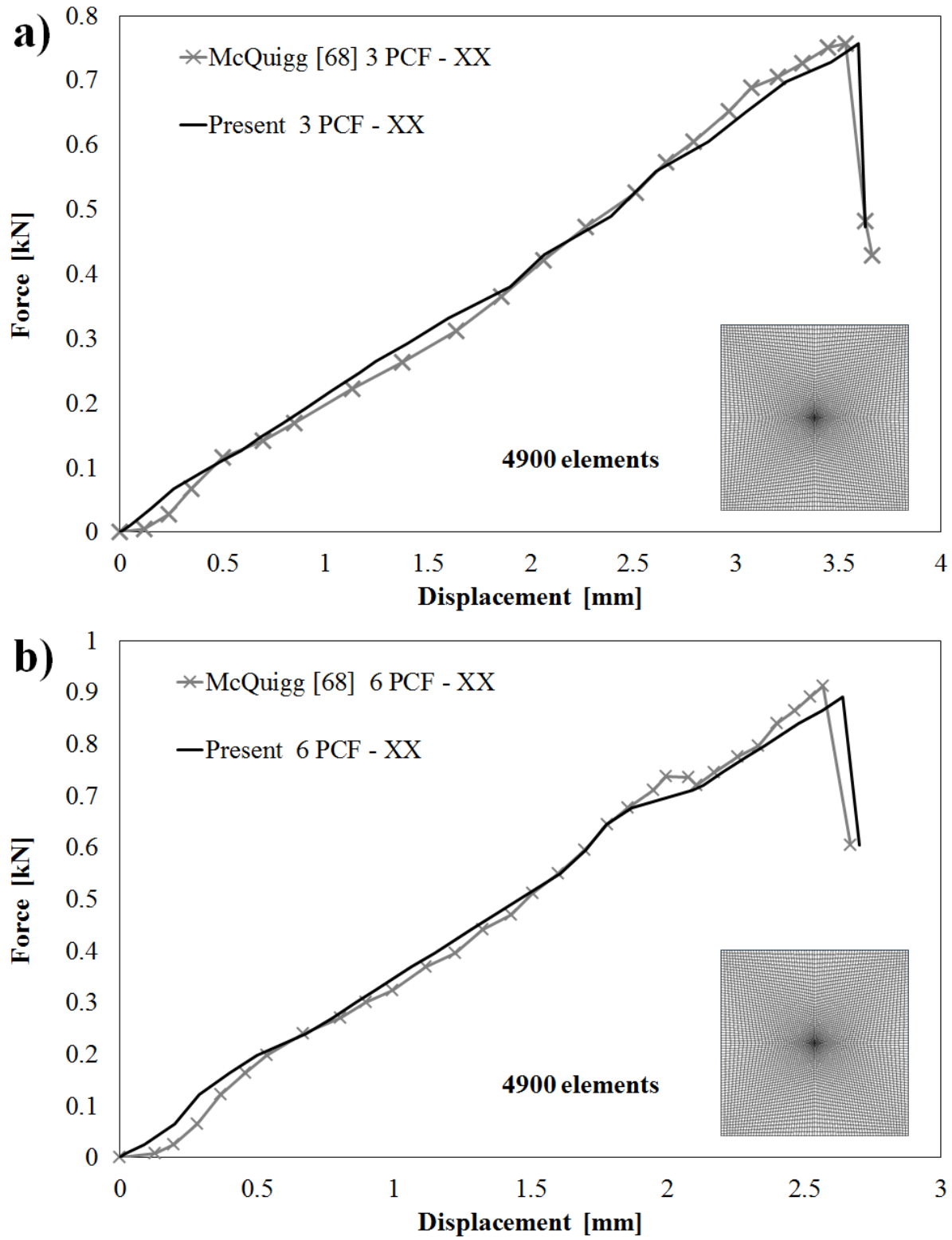

Figure 9. Comparison between experimental force-indentation curves by McQuigg [68] and by the present finite element for sandwich square panel with a) 3PCF honeycomb and b) 6 PCF honeycomb.

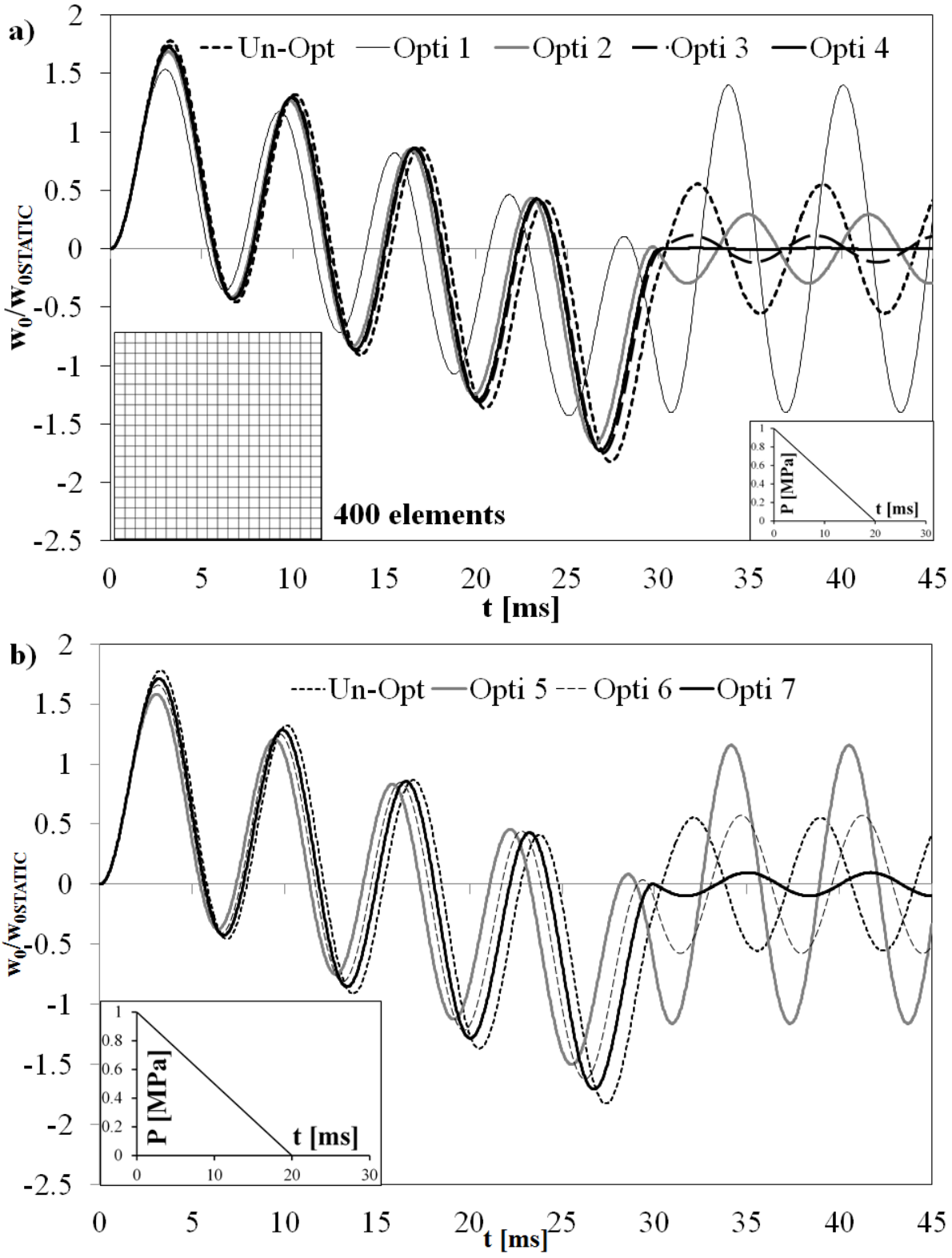

Figure 10. Non-dimensional deflection time history for the optimized lay-ups.

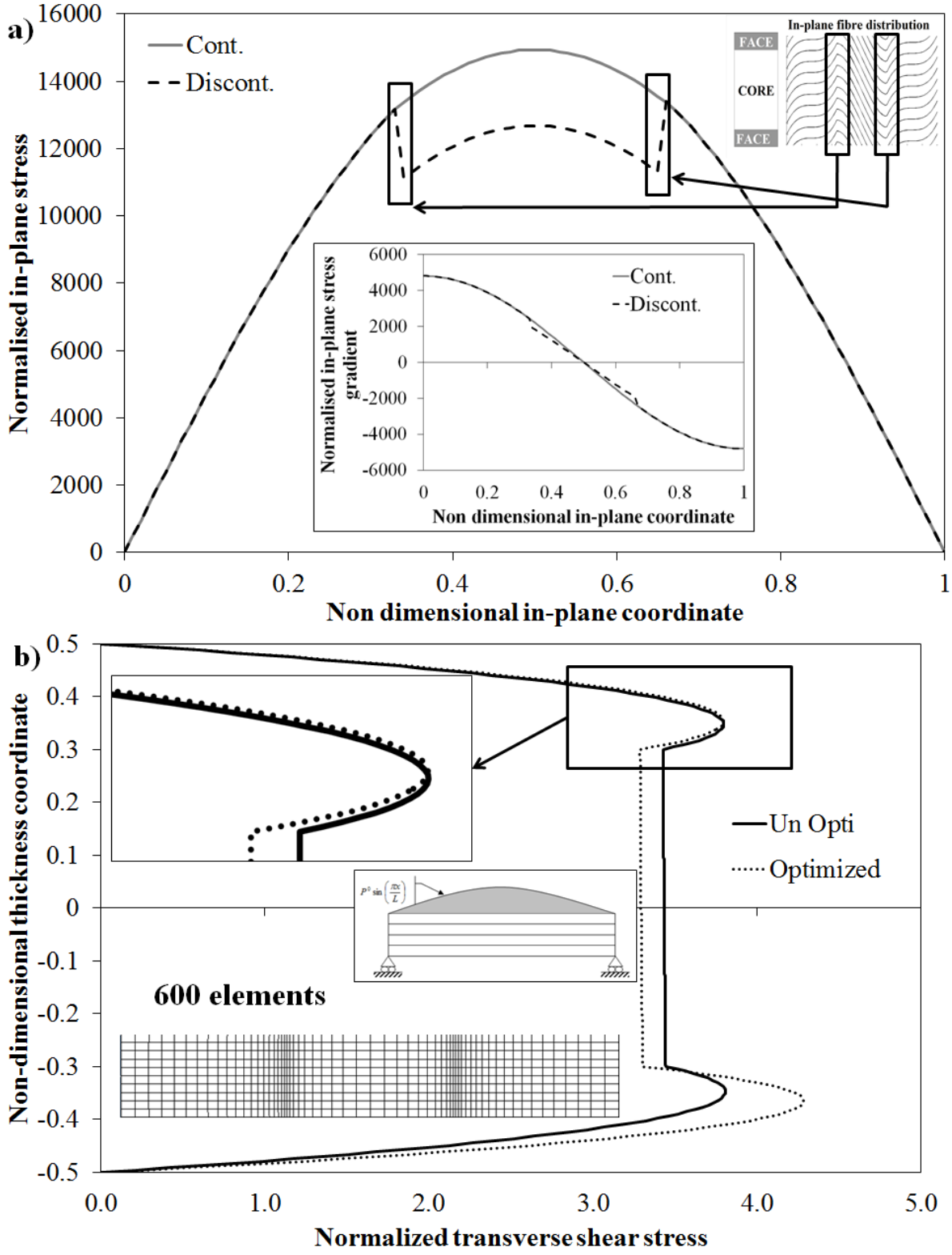

Figure 11. a) In plane variation of the in-plane stress and b) through the thickness variation transverse shear stress for a sandwich beam with step-varying in-plane properties.